Title
MOMENTUM DEPENDENCE OF THE ASYMMETRY IN MUON DECAY

Author
Kruger, Hans.

Publication Date
1961-02-02

UCRL 9322

cy 2

UNIVERSITY OF CALIFORNIA

Ernest O. Lawrence

Radiation Laboratory

MOMENTUM DEPENDENCE OF THE ASYMMETRY IN MUON DECAY

DISCLAIMER

UCRL-9322
UC-34 Physics
TID-4500 (16th Ed.)

UNIVERSITY OF CALIFORNIA
Lawrence Radiation Laboratory
Berkeley, California

Contract No. W-7405-eng-48

MOMENTUM DEPENDENCE OF THE ASYMMETRY IN MUON DECAY

Hans Kruger

(Thesis)

February 2, 1961

Printed in USA. Price $2.00. Available from the
Office of Technical Services
U. S. Department of Commerce
Washington 25, D.C.

MOMENTUM DEPENDENCE OF THE ASYMMETRY IN MUON DECAY

Table of Contents

Table of Contents (cont'd)

MOMENTUM DEPENDENCE OF THE ASYMMETRY IN MUON DECAY

Hans Kruger
(Thesis)
Lawrence Radiation Laboratory
University of California
Berkeley, California

February 2, 1961

ABSTRACT

Positive muons from the Berkeley 184-in. synchrocyclotron were stopped in various materials and the momentum dependence of the asymmetry of positrons from their decay measured with a magnetic spectrometer. The parameters of the polarized muon spectrum, determined by least-squares fitting the theoretical form of the asymmetry to its measured values, are $\rho = 0.774 \pm 0.042$, $\delta = 0.782 \pm 0.031$, $|\xi| \geq R|\xi| = 0.848 \pm 0.036$ for an unrestricted local muon decay interaction, where R is the effective muon-beam polarization. These values of the parameters include radiative corrections and corrections for bremsstrahlung and all instrumental effects.

When the local muon decay interaction with four-component neutrinos is restricted to $g_T = -g'_T$ and to complete positron polarization, these values of ρ and δ imply $|\xi| = 0.989 \pm 0.014$ for any degree of lepton conservation. This value of $|\xi|$ implies that the average muon-beam polarization during this experiment was $R = 0.857 \pm 0.024$. The value $\rho/\delta = 0.985 \pm 0.056$ is obtained independently from the ratio of the asymmetry at $x = 1.0$ and $x = 0.75$, where x is the total positron energy in units of the maximum positron energy. This determination assumes only locality and $|\eta| \ll 1$, and it holds for any degree of lepton conservation.

The smallness of the deviations of the parameters from their values in the local two-component neutrino theory with lepton conservation places an upper limit of about 4% on a possible violation of the lepton-conservation rule, or restricts the radius of a possible nonlocal interaction propagated by intermediary particles to $(0.54 \pm 0.90) \times 10^{-13}$ cm and the

mass of these particles to $\gtrsim 220$ Mev. Thus the measured parameter values are compatible with a local two-component neutrino theory with complete lepton conservation and with 100% positron polarization, i.e. the V - A interaction. For this interaction the measured value of $R|\xi|$ implies $|\eta| \lesssim 0.27 \pm 0.03$.

I. INTRODUCTION

The parameter ρ of the positron spectrum from the decay of unpolarized muons had already been measured by several methods[1-3] when the realization of parity nonconservation necessitated the introduction of two more parameters into the theory in order to complete the description of the decay of polarized muons.

The measurement of the new parameters was made more difficult than that of ρ by the reduced intensity of muons from the decay in flight of pions needed for their determination relative to the intensity of muons from stopped pions available from accelerators. This caused experimenters to focus their efforts on ξ for which a lower limit dependent on the muon beam polarization and depolarization effects could be determined from the energy-integrated spectrum of polarized muons. Garwin, Lederman, and Weinrich[4] reported the first of these measurements, while the most recent was made by Lynch, Orear, and Rosendorff.[5] It was also Garwin and his collaborators who investigated the energy dependence of the asymmetry of positrons from the decay of polarized muons for the first time.[6] Other references to investigations dealing with the muon decay are listed at the end of Section X.

The experiment reported here was designed to permit a thorough measurement of all three parameters from stopped muons by using a magnetic spectrometer as a momentum analyzer with particular emphasis on the δ parameter. It was performed in two separate runs. The results of the first run have already been published in preliminary form.[7] In the meantime a similar experiment was carried out with a hydrogen bubble chamber by Plano.[8]

II. THEORY

For positive muons at rest with longitudinal polarization, R, at the moment of decay, the spectrum of right-handed positrons is taken as[9]

$$N_p \equiv \frac{dN}{dx\, d(\frac{\Omega}{4\pi})} = 2x^2 \left\{ 3(1-x) + 2\rho\left(\frac{4}{3}x - 1\right) - R\xi\cos\theta\left[1-x + 2\delta\left(\frac{4}{3}x - 1\right)\right]\right\}. \quad (1)$$

Here x is the positron momentum in units of the maximum positron momentum, $W = \frac{1}{2} M_\mu = 52.86$ Mev (positron rest mass is neglected); θ is the angle between muon spin and positron momentum; and Ω is the positron solid angle. The parameters ρ, δ, and ξ are given by their usual definitions in terms of the muon decay coupling constants.[10]

The term of the polarized spectrum involving the second Michel parameter η and terms proportional to the square of the positron mass are neglected in Eq. (1). The complete spectrum is[11]

$$N_p \sim E\sqrt{E^2-M^2}\left\{3(W-E) + 2\rho\left(\frac{4}{3}E - W - \frac{1}{3}\frac{M^2}{E}\right) + 3\eta\frac{M}{E}(W-E) - R\xi\cos\theta\frac{\sqrt{E^2-M^2}}{E}\left[W-E + 2\delta\left(\frac{4}{3}E - W - \frac{1}{3}\frac{M^2}{E}\right)\right]\right\}.$$

Here M is the positron mass, E is the total positron energy, $W = (M_\mu^2+M^2)/2M_\mu$ is the maximum total positron energy, and

$$\eta = \frac{(k_{SS} - k_{pp}) - 2(k_{VV} - k_{AA})}{(k_{SS} + k_{pp}) + 4(k_{VV} + k_{AA}) + 6k_{TT}},$$

with $k_{ij} = g_i g_j^* + g_i' g_j'^*$ $(i, j = S, V, T, P, A)$.

The neglect of η is justified because the third term becomes important only at energies lower than those considered in this experiment as long as $\eta \ll 1$. This condition can be assumed to be satisfied, since obviously $\eta \equiv 0$ for the (V-A) theory, and any deviations from this theory are expected to be small. The results of this experiment confirm that these deviations are indeed small.

The assumption contained in Eq. (1) is that the muon-decay Hamiltonian be given its usual local form.[12] The relative magnitude of the different coupling constants has not yet been fixed.

By setting $R = 0$; we obtain from Eq. (1) the positron spectrum for unpolarized muons,

$$N_u \equiv \frac{dN}{dx} = 2x^2 \left\{ 3(1-x) + 2\rho\left(\frac{4}{3}x - 1\right) \right\}. \qquad (2)$$

Figure 1 shows the functional dependence of N_p and N_u on x when the values of the (V-A) theory are assigned to the parameters ($\rho = \delta = 3/4$, $\xi = -1$), the muon beam is completely polarized ($R = 1$), and the decay electrons are observed along a direction parallel to the muon momentum and hence antiparallel to the muon spin ($\cos\theta = -1$), since the positive muon is believed to be left-handed.[13] The normalization common to both spectra was conveniently so chosen as to make $N_u = 1$ at $x = 1$ for $\rho = 0.75$.

The difference between the two spectra expressed as a fraction of the unpolarized spectrum,* Δ, is a useful relation for determining the muon-decay parameters from experimental spectrum measurements:

$$\text{Asymmetry} \equiv \Delta \equiv \frac{N_u - N_p}{N_u} \qquad (3)$$

Substitution of Eqs. (1) and (2) in (3) gives

$$\Delta = R\,\xi\cos\theta\,\frac{1-x+2\delta\left(\frac{4}{3}x-1\right)}{3(1-x)+2\delta\left(\frac{4}{3}x-1\right)} \xrightarrow[\delta = 0.75]{\rho = 0.75} -R\,\xi\cos\theta\,\frac{1-2x}{3-2x}. \qquad (4)$$

*In this report the positron spectrum from the decay of unpolarized muons is N_u. The polarized muon decay spectrum is N_p.

Figure 1 shows the behavior of Δ for the case of the (V-A) theory with $\xi = -1$ and $R \cos\theta = -1$. While a comparison over the entire range of x of the experimentally determined asymmetry with its theoretical form for any chosen set of parameter values will be a measure of the over-all goodness-of-fit of this choice, a comparison at the following fixed energies will also yield information about the individual parameters, if one assumes the spectra to have the forms of Eq. (1) and (2):

(a) At $x = 0.75$, we have

$$\Delta = R\xi \cos\theta \left(\frac{1}{3}\right)$$

and therefore

$$R\xi = 3 \frac{\Delta_{x=0.75}}{\cos\theta} .$$

That is, the asymmetry at this energy measures the product of ξ and R, the muon longitudinal polarization at the instant of decay, which is the product of the longitudinal polarization of the incident muons and all effects contributing to their depolarization after coming to rest. Since we always have $R \leq 1$, $3(\Delta/\cos\theta)$ is a lower limit for ξ. This determination of $R\xi$ is evidently independent of ρ and δ.

(b) At $x = 1.0$, we have

$$\Delta_{x = 1.0} = R\xi \cos\theta \frac{\delta}{\rho}$$

and therefore

$$\frac{\delta}{\rho} = \frac{\Delta_{x = 1.0}}{R\xi \cos\theta} = \frac{\Delta_{x = 1.0}}{3\,\Delta_{x = .75}} .$$

The difference between the measured values of the parameters and their values in the two-component theory can be used to place an upper limit on a possible violation of the lepton conservation rule or on the radius of a possible nonlocal interaction within the framework of the two-component neutrino theory. This possibility is explored in Section VII.

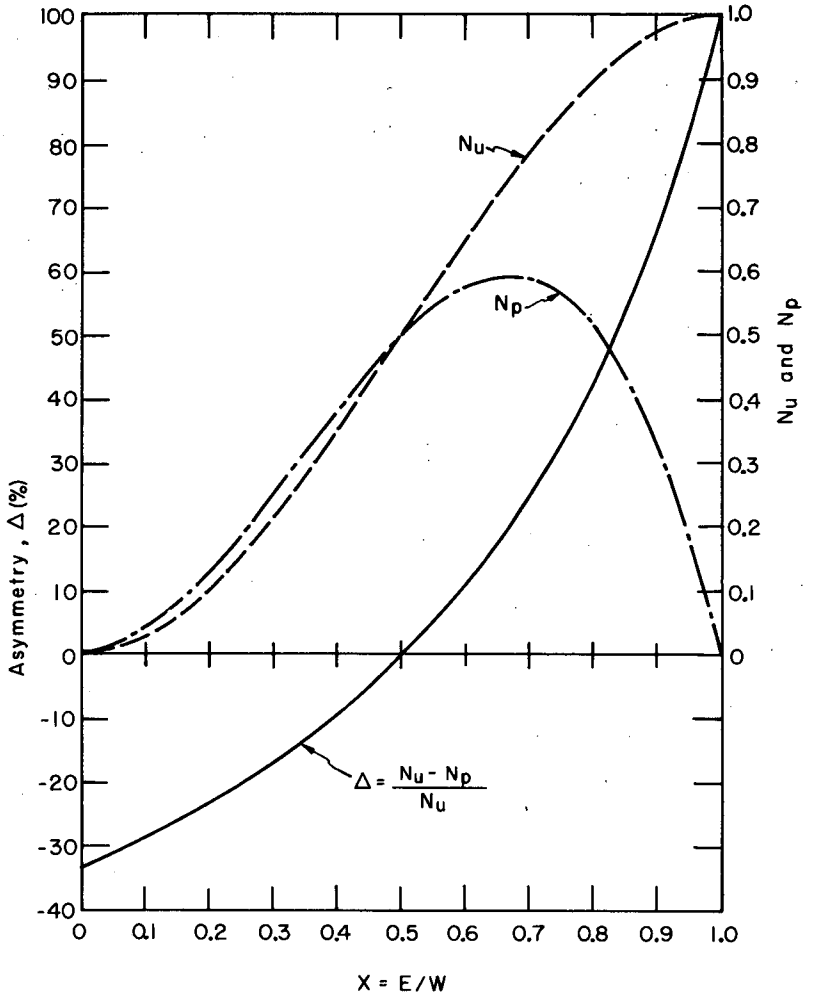

Fig. 1. Unpolarized (N_u) and polarized (N_p) positron spectra from the decay of 100% polarized muons at rest for $\theta = 180$ deg as given by the (V-A) theory. The asymmetry is $\Delta = (N_u - N_p)/ N_u$; the maximum positron energy is W = 52.86 Mev.

The asymmetry, Δ, is relatively insensitive to η as is indicated by the following numerical example: Changing η from 0 to 0.1 decreases Δ by 0.8% at E = 10 Mev (the lowest positron energy of this experiment) and by 0.3% at E = 25 Mev. The dependence of Δ on η decreases with increasing energy. The asymmetry at the maximum energy is independent of η.

III. EXPERIMENTAL METHOD

The polarized spectrum can be measured along any direction but the normal with respect to the muon beam. Since the asymmetry is proportional to $\cos\theta$, the angle θ should be as small as possible.

There exist three possibilities for measuring the unpolarized spectrum: (a) The line of observation could be placed at 90 deg with respect to the muon beam, which would require alternating between two positions when alternating between N_u and N_p measurements; (b) two different sets of equipment could be built--one for each direction of observation--and N_u and N_p could be measured simultaneously; (c) the muons could be depolarized by precessing them in a magnetic field thus permitting observation of both spectra along the same direction. Since it is desirable in a measurement of this degree of accuracy to alternate frequently between N_u and N_p measurements in order to average over fluctuations in the cyclotron operation, and as equipment duplication would introduce different efficiencies into the measurements of the two spectra, the latter method was chosen. In this method the precession coils can also be used for the necessary cancellation of the cyclotron stray field at the location of the muon stoppers for the observation of the polarized spectrum.

The positron spectrum from the decay of muons at rest in a magnetic field which causes the muon spin to precess with angular frequency ω, for a fixed observation angle, θ, is

$$\frac{dN}{dx\, d\left(\frac{\Omega}{4\pi}\right)} = \int_0^\infty 2x^2 \left\{ G_1(x,\rho) - R\xi\, G_2(x,\delta)\cos(\theta \pm \omega t) \right\} e^{-t/\tau}\, d\left(\frac{t}{\tau}\right), \quad (5)$$

where

$$G_1(x,\rho) \equiv 3(1-x) + 2\rho\left(\frac{4}{3}x - 1\right),$$

$$G_2(x,\delta) \equiv 1 - x + 2\,\delta\left(\frac{4}{3}x - 1\right),$$

and

$$\tau = \text{muon life time} = 2.22\times10^{-6}\ \text{sec.}$$

The normalization is that used in Eq. (1) of Section II. The plus(minus) sign of ω applies when the initial spin precession tends to increase (decrease) the angle between muon spin and electron momentum. Integration results in

$$\frac{dN}{dx\, d(\frac{\Omega}{4\pi})} = 2x^2 \left\{ G_1 - R\,\xi \cos\theta\, G_2\, F(\omega) \right\}, \tag{6}$$

with

$$F(\omega) \equiv \frac{\tau^{-2} \pm \tau^{-1}\,\omega\,\tan\theta}{\tau^{-2} + \omega^2} .$$

One sees that:

$$\text{(a)}\quad \frac{dN}{dx\, d(\frac{\omega}{4\pi})} = N_p \tag{7}$$

for $F(\omega) = 1$, i.e., for $\omega = 0$ or the singular values $\omega = \mp \frac{\tan\theta}{\tau}$;

$$\text{(b)}\quad \frac{dN}{dx\, d(\frac{\omega}{4\pi})} = N_u \tag{8}$$

for $F(\omega) = 0$, i.e., for $\omega = \infty$ or the singular values $\omega = \pm \frac{1/\tau}{\tan\theta}$.

Case (a) corresponds to not precessing the muon spin at all or precessing with a period so very much larger than the muon lifetime that essentially all muons have decayed before the spin has turned through an appreciable angle. Case (b) applies to a muon the spin of which is turning so quickly that in the span of a few muon lifetimes the spin points in all directions with equal probability and therefore the positron decay pattern is isotropic.

The experimental method for identification of positron momentum employed a scintillator matrix array for the definition of trajectories in a magnetic spectrometer and a target-counter sandwich that defined the positron energy loss. This method provided maximum intensities by permitting the use of targets sufficiently thick to stop most of the muon beam and the use of the full spectrometer aperture without sacrificing adequate momentum resolution.

IV. EXPERIMENTAL EQUIPMENT

Experimental Set-Up

This experiment was performed in two separate runs which will be designated in chronological order by I and II. The instrumentation for the individual runs was identical in principle but differed in some details, which will be explained below.

The positive π-meson beam used in all runs was produced in an internal Be target bombarded in the 184-in. synchrocyclotron. After leaving the vacuum tank through a thin window, the beam passed through an 8-in.-bore quadrupole doublet, Q_1 (Fig. 2), and an 8-ft-diam iron collimating wheel having a bore of 7-1/2-by-12-in. section. It was then deflected through 30 deg by magnet M1 which was fitted with a strong-focusing pole piece. The 12 in. bore quadrupole, Q2, through which the beam then passed was used only during beam studies in the early stages of the experimental but not during the data runs because the focusing action of the quadrupole was found to depolarize the muon beam. For the same reason, Q_1 was used only for beam studies. The beam was deflected 47 deg by magnet M2 before it was slowed down by a thickness of carbon degrader sufficient to stop it in a sandwich of alternate layers of scintillation counters and target material. The decay positrons were then momentum-analyzed by a magnetic spectrometer. Collimators before and after the degrader prevented particles in the direct meson-beam from entering the spectrometer when it was in its forward position.

The materials and thicknesses of the targets used in the three different runs are listed in Table I.

The target-counter sandwich was centered on the spectrometer center line, each target and counter being parallel to the spectrometer pole face. The data were taken with the spectrometer placed in one of two positions. In the forward position (shown in Fig. 2), the spectrometer is turned until its optical axis and therefore the average positron momentum forms an angle, α, of a few degrees with the beam axis in order to minimize background counts. This position yields the

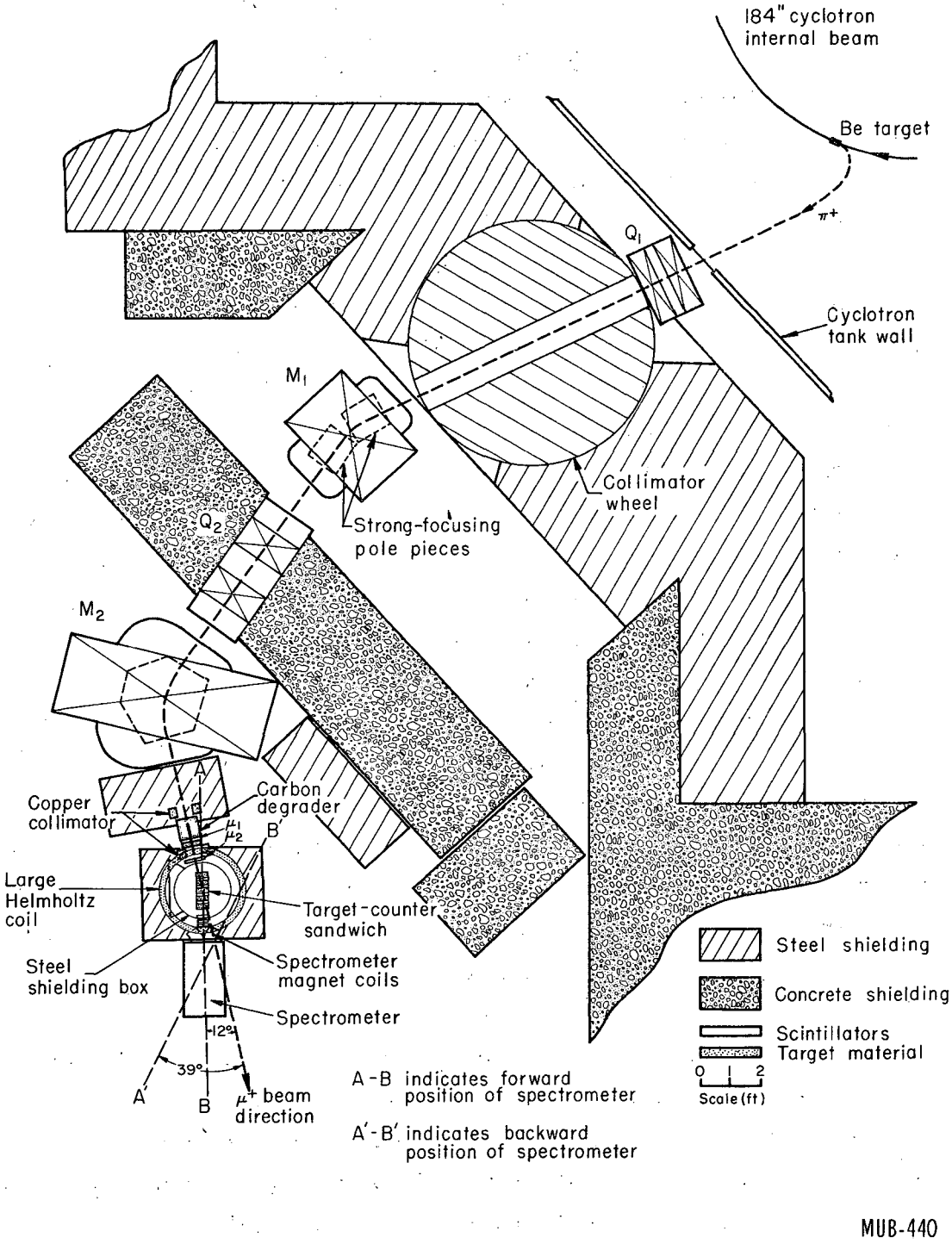

Fig. 2. Experimental setup in the meson-beam cave of the Berkeley 184-in. synchrocyclotron.

largest possible asymmetry, but the background is higher than it would be for a backward position. For this reason in this position measurements were made mostly at high positron momenta which are associated with large spectrum yields. Since the positive muon is left-handed,[13] θ is 180 deg - α. In the backward position, which is indicated by the line A'B' in Fig. 2, the smallest angle θ to which the spectrometer could be turned before the pole face began interfering with the beam was 39 deg. All low-momentum runs of Experiment II were taken in this position. The values of θ for each run are listed in the tables.

Meson Beam

The characteristics of the positive-meson beam of the 184-in. synchrocyclotron during Run II are typical for the entire experiment.

When the beam entered the degrader it had the particle-range distribution shown in Fig. 3, which indicates a π^+-to-μ^+ ratio of about 7:1. This figure also shows the method by which the range curve was measured. During the range-curve measurement, the beam intensity was reduced to one-tenth of the maximum beam in order to prevent saturation of the coincidence circuit.

The position of the peaks of the differential range curve gives the average pion momentum as 210±5 Mev/c (a range of 35.4±2.5 g/cm^2 in carbon) and that of the muons as 212±10 Mev/c, since the fixed amount of carbon was 2.94 g/cm^2, and the equivalent carbon thickness of counters μ_1 and μ_2 was 0.87 g/cm^2. In this calculation the full 1/4-in. thickness of the scintillator μ_1, but only half the thickness of μ_2 was used. It is assumed that the energy lost by the mesons in traversing 1/8 in. of plastic scintillator yields a pulse height sufficiently large to produce a coincidence output.

The pion contamination of the beam stopping in the targets at muon range for negative pions was measured in the course of a different experiment.[14] In that experiment the prong distribution found in Ilford G-5 emulsions which had been exposed at the target position behind a degrader thickness of 43.2 g/cm^2 of carbon was compared with the known

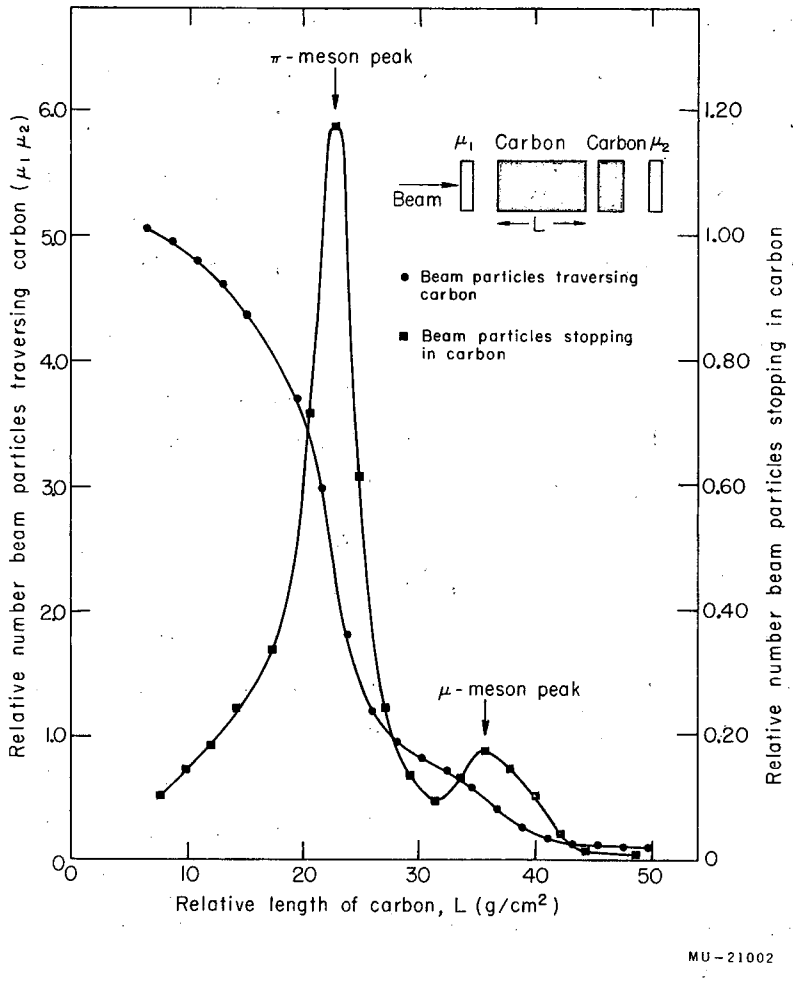

Fig. 3. Range curve of the meson beam. The absolute scale for the left abscissa is 10^6 per minute and that for the right abscissa is 10^6 per minute per 2.2 g/cm^2 carbon stopper.

prong distributions of π- and μ-produced stars. This measurement gave about 0.5% as a conservative upper limit. This value will also be valid for the positive meson beam. Because the degrader used during this experiment was even thicker, the actual pion contamination was considerably less than this value.

The maximum meson beam intensities obtained during the experiment are indicated in Fig. 3. The absolute scale for the left abscissa is 10^6 per minute and that for the right abscissa is 10^6 per minute per 2.2 g/cm^2 carbon stopper.

Magnetic Shielding and Precession Coils

The following paragraph lists the dimensions of the Helmholtz coils which are shown in Figs. 2 and 4. During Run II a Helmholtz-coil set of 37-in. mean diameter and 15-1/2-in. separation between coils provided the magnetic fields for cancelling the stray cyclotron field of about 50 gauss at the target position. A coil set of 10-1/4-in. mean diameter and 12 in. separation supplied the precession field. During Run I the smaller coil was used for both purposes. Both coils were wound of 1/16-by-1/2-in. copper strips.

The smaller coil was mounted on the bottom and lid of a cylindrical soft-iron box. The box, which was 13 in. high with an inner radius of 10 in. and 1/4-in. walls, had been designed mainly as a static magnetic shield for Run I. It also served as a permanent support for the target holder and scintillator assemblies during both runs.

The Helmholtz-coil field during the N_0 measurement ranged among the target positions from zero to 0.71 gauss in Run I and from 0.16 to 0.54 gauss in Run II. During the $N_\downarrow$ measurements this range was 56.1 to 57.2 gauss for Run I and 57.2 to 61.3 gauss for Run II.

Magnetic Spectrometer

The positrons from the decay of muons in the target-counter sandwich passed through a 180 deg, 18-in. mean radius, n = 1/2 (and therefore double-focussing) magnetic spectrometer. Figure 4 is a scale drawing of the spectrometer's location relative to the muon targets, while Figs. 5 and 6 give all essential engineering details of the spectrometer.

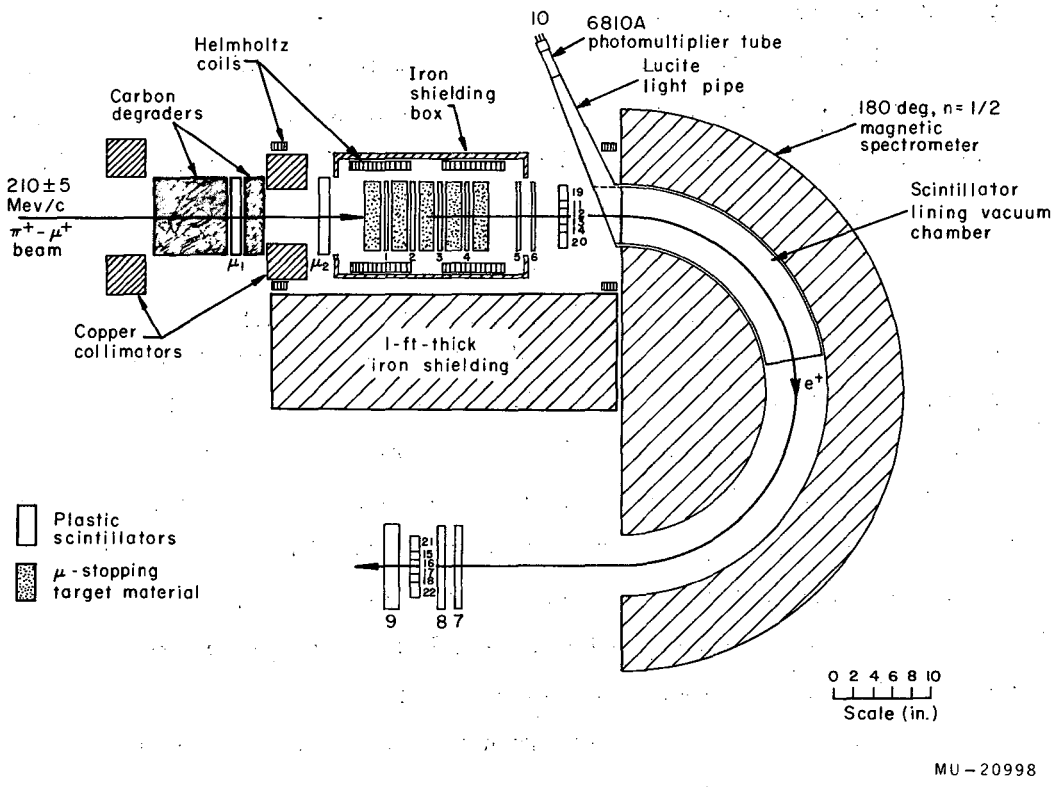

Fig. 4. Side view of experimental equipment in the immediate vicinity of the magnetic spectrometer.

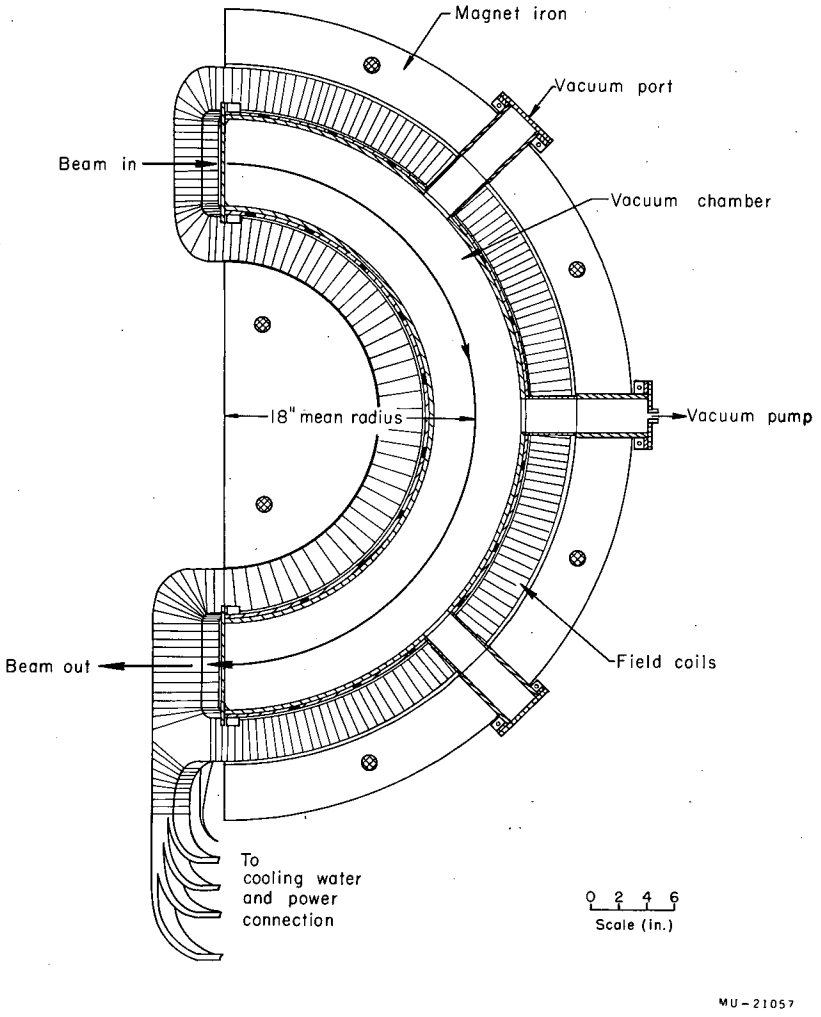

Fig. 5. Section through the median plane of the magnetic spectrometer.

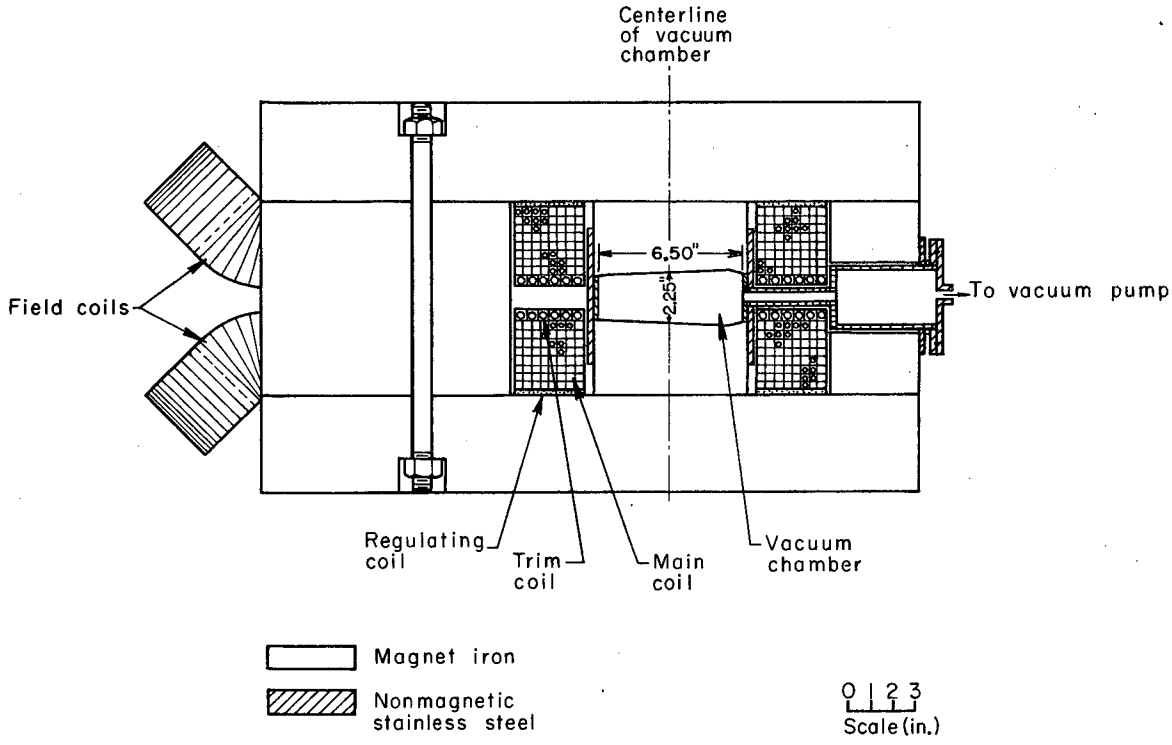

Fig. 6. Radial section through the spectrometer vacuum chamber.

Many authors have contributed to the development of the theory of this type of spectrometer, and one of the more recent articles dealing with this subject is that of Judd.[15] Using Judd's results, one computes a fractional solid angle for the vacuum chamber cross section of 6-in. radius and 2.25-in. average height used in this experiment as 0.13% for a source distance of 19.5 in. This was the typical separation between the center of the target-counter sandwich and the spectrometer pole face. The average radial and vertical magnification was 1.26.

The calculated momentum-resolution function of this instrument for a 1-in.-high source slit (i.e. the extent along the spectrometer radius at the entrance or exit aperture) and a 1.26-in.-high detector slit located at conjugate foci on the optical axis is given by the fold of two rectangles of equal heights and of widths $\Delta p = (1.549\%)\, p_0$, where p_0 is the momentum corresponding to a trajectory of radius equal to the mean radius of 18 in. Thus the resolution function is an isosceles triangle of full width at half-maximum equal to this Δp.

The spectrometer field is a linear function of the current to better than 0.1% over the range of energies of this experiment. The vacuum chamber was pumped out during all runs, thus minimizing the effect of air-scattering on intensity and resolution. The chamber was sealed with 2-mil mylar windows.

Scintillation Counters

Figure 4 shows all the scintillators used during Run II. The chemical composition of the scintillating plastic is typical of all scintillators produced by the Lawrence Radiation Laboratory at Livermore: 97% polystyrene, 3% terphenyl, and 0.03% tetraphenyl butadiene. The density was 1.05 g/cm^3. The thickness, height, and width in inches were, respectively: μ_1 and μ_2, 0.250 by 8 by 8; β_1 to β_5, 0.0333 by 4 by 7.5; β_6, 0.0625 by 4 by 7.5; β_7 and β_8, 0.125 by 4 by 9; β_9, 0.250 by 4 by 9; β_{11} to β_{14}, 0.125 by 0.750 by 3; β_{15} to β_{18}, 0.125 by 0.945 by 3; β_{19} and β_{20}, 0.125 by 1.500 by 3; β_{21} and β_{22}, 0.125 by 1.890 by 3.

The height of any pair of counters defining the radius of curvature of the positrons in the spectrometer determined the momentum resolution.

The ratio of the heights of entrance-matrix counters β_{15} through β_{18} relative to exit matrix counters β_{11} through β_{14}, and of entrance matrix counters β_{19} and β_{20} relative to exit matrix counters β_{21} β_{22} reflected the magnification of the spectrometer. Entrance and exit matrix counter sets were located at conjugate spectrometer foci. All counters utilized RCA 6810 or 6810A photomultiplier tubes.

The target-dividing counters β_1 to β_4 were made as thin as feasible in order that the ratio of muons stopping in the scintillating plastic to those coming to rest in the targets could be kept at a minimum (1:10 during Run II). Positrons from the decay of muons stopped in scintillators would show an asymmetry reduced by a factor of 0.35 relative to lithium.[16] For the same reason 1/4-mil-thick aluminum foil scintillator wrapping was chosen.

Run I differed from Run II only in the number of target-dividing counters (three instead of five: β_1, β_2, β_3) and in the absence of the matrix counters. In the part of Run I during which a carbon target was used, target-dividing counters were not utilized at all.

The counter β_{10}, which lined an 80-deg sector of the spectrometer vacuum chamber beginning at the entrance aperture, was used in both runs. Figure 7 shows the construction of this counter. The large sides of the scintillator body were 0.125-in-thick sections of a ring of 14.75-in. inner and 21.25-in. outer radius. The small sides were 0.250-in. thick. All surfaces were machined to fit the contour of the vacuum-chamber inner walls. The light was conducted to the photomultiplier tube by a lucite rod. The diameter of the rod which was 1.75-in. o.d. at the photomultiplier tube gradually increased to permit a smooth transition to the 2.5-by-4-in. side of the lucite box of 0.25-in. average wall thickness. Optical contact between this box and the scintillator lining was made through the mylar vacuum chamber window and a lucite frame which held the scintillator to the pole face.

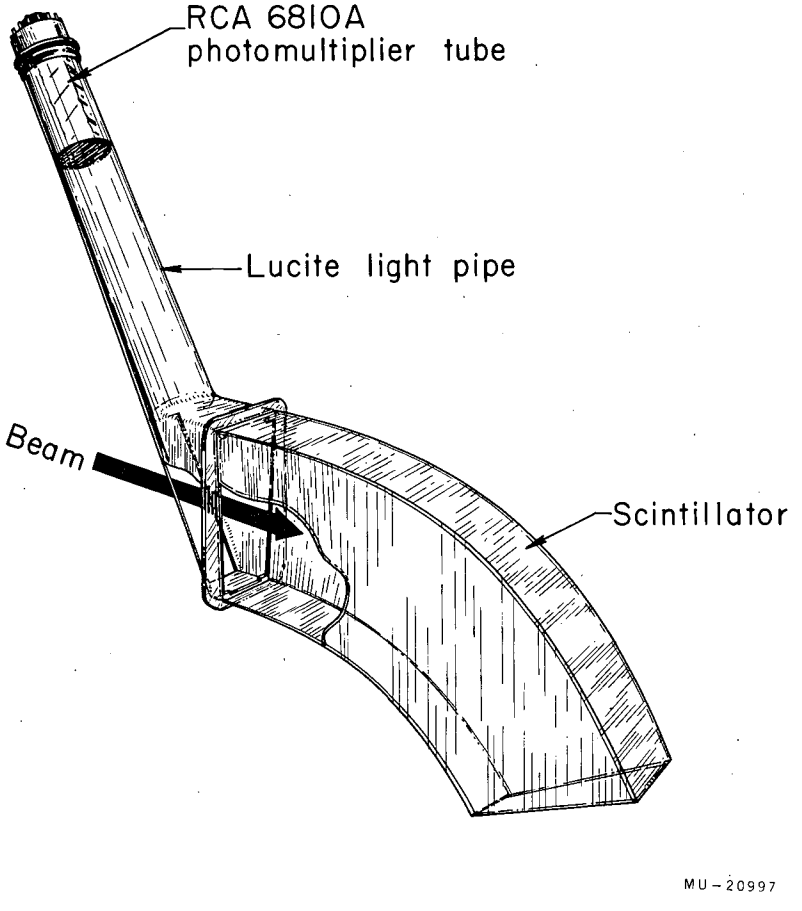

Fig. 7. View of scintillation counter that lined the upper half of the spectrometer vacuum chamber. The opening in the lucite light pipe, through which the beam enters, is also lined with scintillator.

It was the function of this scintillator lining to supply an anti-coincidence signal for all positrons that scattered off the vacuum-chamber walls during their passage through the spectrometer. A 0.0625-in. thick scintillator lining on the inside of the lucite light-pipe box provided such a signal also for all positrons that were scattered by this box. The effect of wall-scattering would be mainly an upward distortion of the muon decay spectrum, especially at lower energies. Figure 8 shows the effectiveness of the β_{10} anticoincidence counter in reducing this effect in the measurement of the unpolarized spectrum. The 6810A phototube of the β_{10} counter was operated at 2300 v, which placed it well on its voltage plateau. To check the light-collection efficiency of the β_{10} counter, a small source of minimum-ionizing electrons was placed at various positions inside the scintillator lining, and the pulse height of the phototube output was measured. The pulse height was found to be independent of the source position in the first 40 deg of the lining, while it dropped by a factor of 3.5 in the next 40 deg. During the experiment, the β_{10} output, which was amplified by two Hewlett Packard amplifiers, was saturated.

Electronics

The operational logic of the electronic circuits used in this experiment is indicated in Fig. 9. Circuit details are shown in Fig. 10.

The double coincidence (μ_1 μ_2) monitored the meson beam. A positron that properly passed through the spectrometer was signaled by the cascaded coincidence $(\overline{\mu}_2\beta_6\beta_7\beta_8)=\beta_A$ and $(\overline{\mu}_1$ or $\overline{\beta}_{10}$, $\beta_A\beta_5\beta_9)=\beta_B$. The β_B coincidence rate represented the sum of the yields from all targets. Any one target could be identified as the origin of a decay positron by requiring a coincidence between β_B and the target-dividing counter behind this target in anticoincidence with all target-dividing counters preceding it. For instance, the positron yield from Target 4, which will be denoted by T-4, was the ($\overline{\beta}_1$ or $\overline{\beta}_2$ or $\overline{\beta}_3$, $\beta_4\beta_B$) coincidence output.

All fast-coincidence circuits used for these operations during Run II were of the Wenzel type, while during Run I they were of the Evans and Garwin types.[17] G7A diodes were used for cascading the β_1 through β_4 anticoincidences.

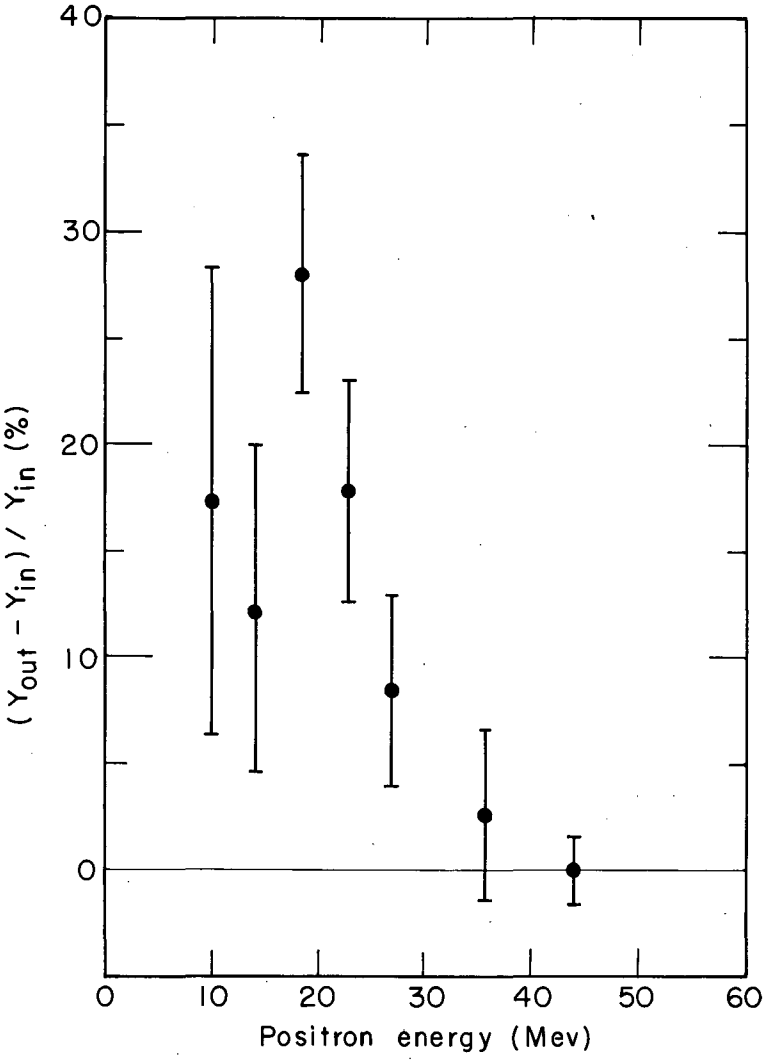

Fig. 8. Effect of the vacuum-chamber scintillator lining on the unpolarized spectrum. Here Y_{in} is the β_B yield when this counter is connected as an anticoincidence signal, and Y_{out} is the β_B yield when it is not connected.

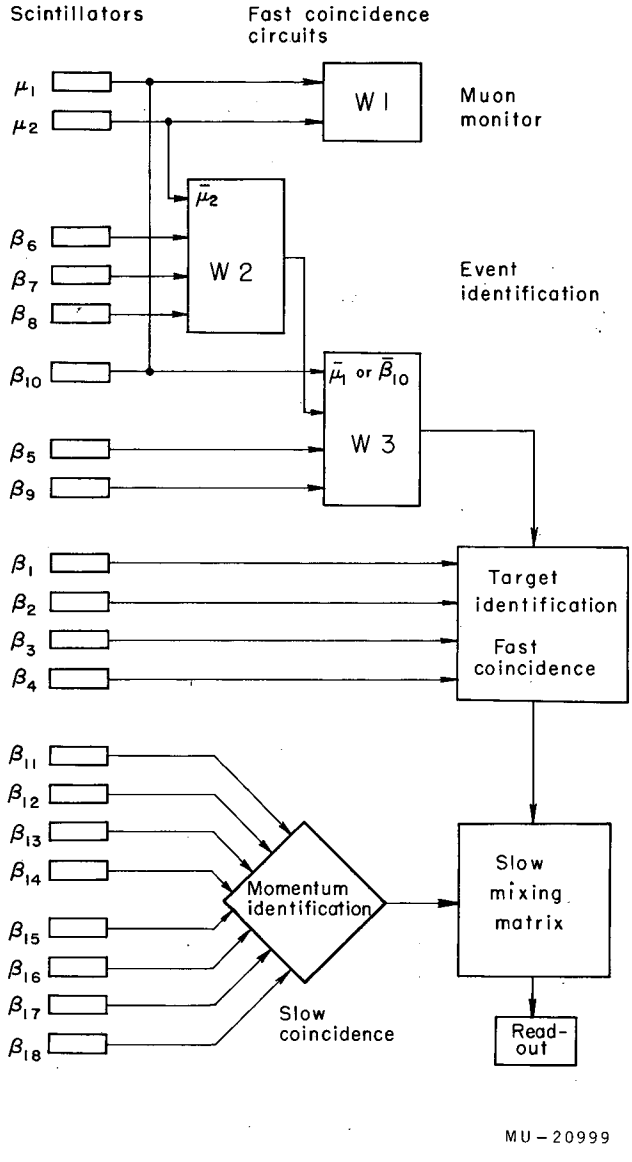

Fig. 9. Operational logic of the electronics used in this experiment.

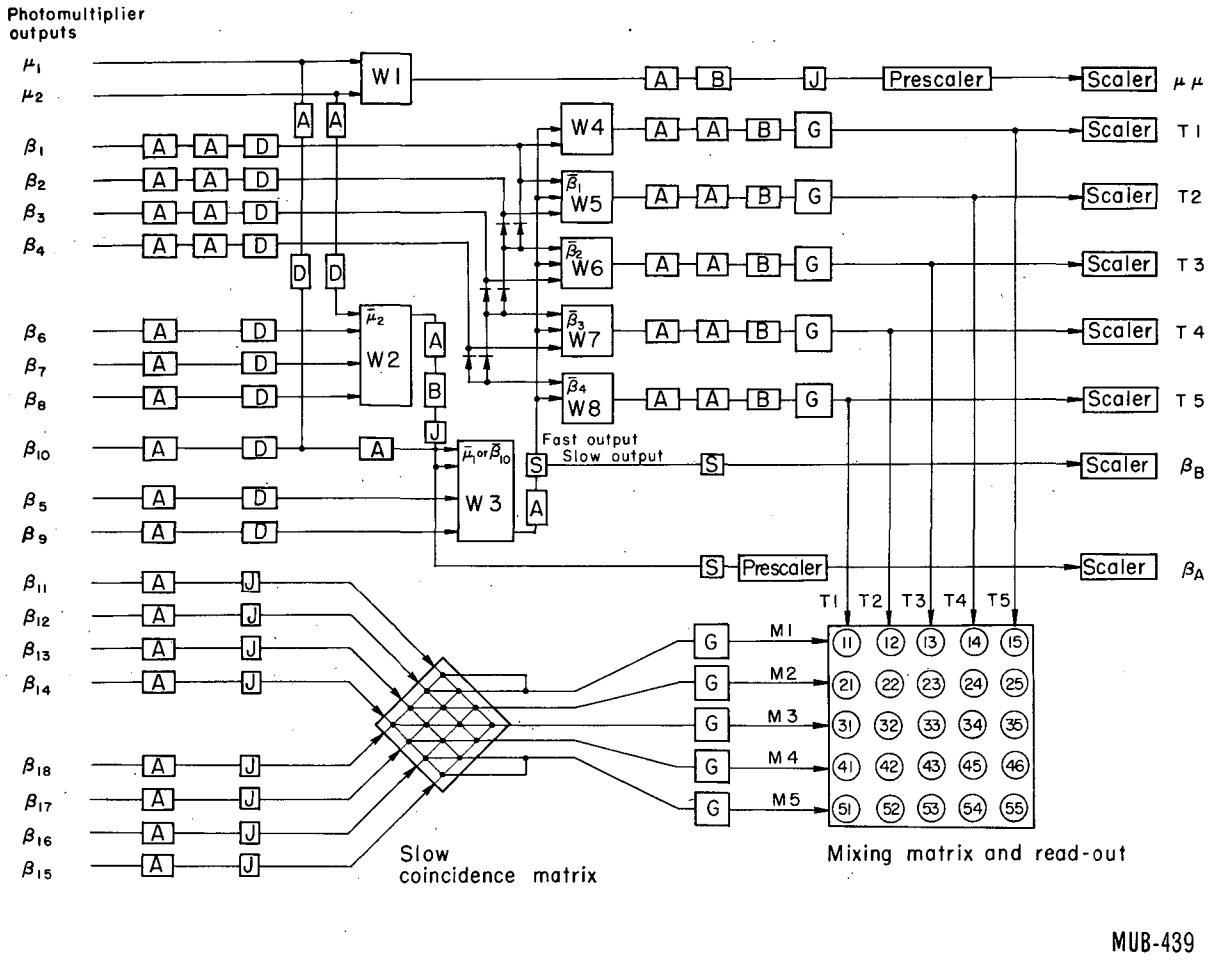

Fig. 10. Circuit details. Here A and B are Hewlett-Packard 460A and 460B distributed amplifiers, D indicates variable delays, J indicates Mey discriminators, S indicates Swift discriminators, W denotes Wenzel fast-coincidence circuits, C denotes variable gate and delay units, and the prescaler is a Hewlett-Packard Model 520A. For details see reference 17.

The matrix-counter design permitted the momentum resolution to be adjusted by a factor of two: Either any of the counters β_{11} to β_{18} could be used as inputs for the four-by-four coincidence matrix or the outputs of two neighboring counters in this group could be added to provide twice the yield at half the resolution. The latter was done in this experiment, so that the matrix inputs labeled as β_{11}, β_{12}, β_{13}, β_{14}, β_{15}, β_{16}, β_{17}, and β_{18} in Fig. 10 actually were the counter outputs β_{19}, $\beta_{11}+\beta_{12}$, $\beta_{13}+\beta_{14}$, β_{20}, β_{21}, $\beta_{15}+\beta_{16}$, $\beta_{17}+\beta_{18}$, and β_{22}, respectively.

The matrix-counter outputs triggered a Mey-type[17] 10-Mc amplitude discriminator, the 60-nsec outputs of which were fed into a coincidence matrix. This device gave an output for a coincidence between any entrance and any exit matrix counter. Those of the sixteen possible outputs that corresponded to equal radii of curvature were added as indicated in Fig. 10; for instance, M3 was the sum of all coincidence $(\beta_{14}\beta_{18})$, $(\beta_{13}\beta_{17})$, $(\beta_{12}\beta_{16})$, and $(\beta_{11}\beta_{16})$, all being produced by positrons having on the average a radius of curvature equal to the mean spectrometer radius. The coincidences $(\beta_{11}\beta_{18})$ and $(\beta_{14}\beta_{15})$--the largest and the smallest possible radii--which had only a 25% probability of occuring relative to M3, were added to M1 and M5, respectively. The resultant increase in the width of these two momentum bands was small.

Thus the central momenta of the five neighboring momentum bands associated with the added matrix outputs are:

M1 $\quad p = [1+7/3(\Delta p/p)]p_0$

M2 $\quad p = (1+\Delta p/p)p_0$

M3 $\quad p = p_0$

M4 $\quad p = (1-\Delta p/p)p_0$

M5 $\quad p = [1-7/3(\Delta p/p)]p_0$,

where p_0 is the momentum corresponding to an 18in. radius of curvature, and $\Delta p/p = 2.324\%$ is the full width at half maximum of the momentum resolution function of the 1.50-in.-high entrance and 1.89-in.-high exit matrix counters.

The five outputs of the coincidence matrix and of the target-identifying Wenzel circuits W4 to W8 triggered variable-delay and gate units of the Brown type.[17] Their 200-nsec outputs were the inputs of a five-by-five mixing matrix, the 25 outputs of which identified the momentum band and origin target of each event.

V. EXPERIMENTAL PROCEDURE

The polarized and unpolarized spectra were measured in alternate runs of about one-half hour which were interspersed with frequent background measurements during which the targets were removed but the dividing-counters left in their positions. This method of background correction subtracts from the signal rate simultaneously contributions from muons stopping in the dividing counters as well as accidental coincidences. It will be shown in Section VI that the muon-stopping distribution in the counters does not change appreciably when the targets are removed.

Separate measurements of the accidental rate at E = 60 Mev (which corresponds to a momentum band well above the spectrum end) relative to the signal rate at about 48 Mev (the maximum of the unpolarized spectrum) gave for Run II a ratio of 2% for the β_B and 1% for the T rates. For Run I the ratio is about 20% for both rates. Average rates were about 200 per hour for β_B and 40 per hour for T at the spectrum maximum, and 20 per hour for β_B and 2 per hour for T at E = 15 Mev.

The spectrometer trimming coils were aiding the main coils during Run II, but they were not connected during Run I. The spectrometer was calibrated in connection with another experiment, during which the trimming field was aiding the main field, utilizing the end of the positron spectrum from the decay of unpolarized muons produced by pions at rest (Fig. 11). The current at which the spectrum had reached a value equal to one-half its maximum--117.8±0.2 amp--was chosen as the calibration point because it was the least dependent on resolution effects. This current value was shown to correspond to a positron total energy of 50.698 Mev by folding all relevant resolution effects into the theoretical spectrum of the (V-A) theory. This calibration point is also independent of the three spectrum parameters.

The residual field in the spectrometer gap at the central radius normal to the plane containing the optical axis and along the direction of

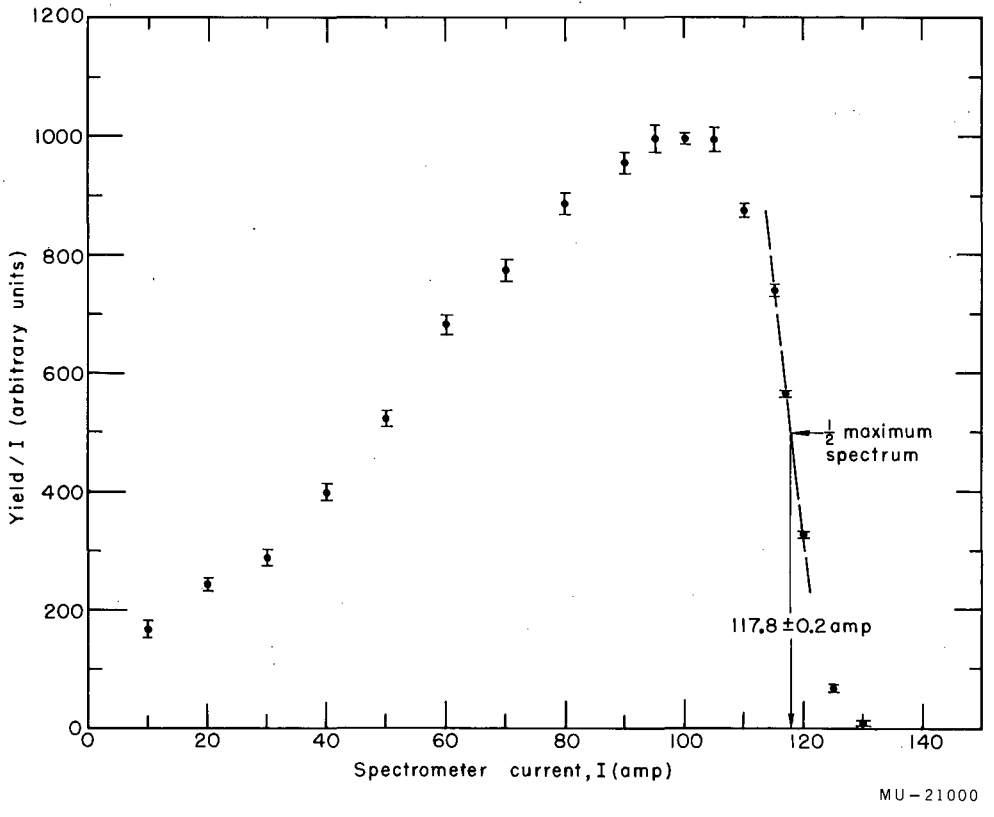

Fig. 11. Positron from unpolarized muons used to calibrate the spectrometer. The yield was divided by the current to remove the effect of the variation with current of the momentum band accepted by the spectrometer.

the main coil field for positrons was measured with a precision rotating-coil gaussmeter as 19.34±0.01 gauss. This leads to the following calibration for Run II:

$$E_s = (0.4282 \pm 0.007)\, I + 0.2652 \text{ (Mev)},$$

where I is the spectrometer current in amperes and E_s the positron total energy.

The calibration constant for Run I (0.3891±0.0016 Mev/amp) was obtained by multiplying that of Run II by a_I/a_{II}, where these constants were determined from a least-mean-squares fit of a straight line B=aI+b to the spectrometer field, B, at the central radius as a function of spectrometer current, I, for both connections of the trimming coils. Here the magnetic field was measured with nuclear-magnetic-resonance equipment. The residual field, b, determined by this method was 31±10 gauss. This error is so large because b could not be measured directly by the nuclear-magnetic-resonance method, but had to be obtained by extrapolation to zero spectrometer current from field measurement at higher currents.

VI. RESULTS AND CORRECTIONS

The raw data is reproduced in Table I. Tables II and III show the asymmetry measured in experiments I and II for the T outputs and mixing matrix outputs, based on a total of about 30,000 events (about 6,200 low-energy events) and lists the necessary corrections. The calculation of these corrections, which are tabulated in Table II, is described below.

Background

Target-out measurements were made with and without a precession field, and the asymmetry was corrected as shown in Appendix A. For a few data runs, background measurements were available with only one orientation of the magnetic field, so that the background had to be treated as being isotropic. The errors due to background were propagated by standard formulas (see Appendix A). The magnitude of the background correction can be obtained from Table III.

The distribution of muon stoppings is not flat over the targets used in this experiment, as can be seen from the range curve (Fig. 3) so that the muon-stopping rate in the dividing counters will change when the targets are removed. The effect of this change on the background-corrected asymmetry is shown in Appendix B to be given by

$$k\left(\frac{\Delta^t}{\cos\theta}\right)\frac{b^t_{\downarrow}}{n_{\downarrow} - b^t_{\downarrow}},$$

where the quantities are defined in the appendix A. For the asymmetry at low energies, this effect vanishes, since we have $(\Delta^t/\cos\theta) \cong 0$, while it is negligibly small at higher energies.

Radiative Corrections

The polarized and unpolarized spectra of the (V-A) theory with the inclusion of radiative corrections as given by Kinoshita and Sirlin[19] were calculated using an IBM 650 computer. The difference between the asymmetry obtained from the new spectra, Δ', and the uncorrected asymmetry, Δ^0, are shown in Table II. One sees that Δ^0 is always less than Δ'.

The use of the (V-A) theory for the calculation of radiative corrections was justified a posteriori by the fact that the parameters obtained from this experiment agree within their errors with the values of the parameters in this theory.

Bremsstrahlung

The sum of the exact Wheeler-Lamb cross-sections for bremsstrahlung in the field of nuclei and of the atomic electrons [19] was folded into the radiation-corrected spectra for each of the target pieces and each target material. The part of this convolution integral for fractional momentum transfers to the photon, κ, between zero and 0.1% was performed with Heitler's [20] integrated cross section, [21] which becomes for $\kappa \ll 1$

$$W(bt, \kappa) = \frac{(\kappa)^{bt}}{\Gamma(bt+1)},$$

where t is the average material thickness in g/cm^2 traversed by the positrons (as given in Table III) and

$$b = \frac{4}{3} L^{-1} = \frac{4}{3}\left\{4\alpha \frac{N}{A} r_0^2 \ln(183\, Z^{-1/3}) Z\left[Z + \frac{\ln(1{,}400\, Z^{-2/3})}{\ln(183\, Z^{-1/3})}\right]\right\} (g/cm^2).$$

The letters in L, the radiation length in the limit of complete screening, have their conventional meaning. This treatment of the integral insures convergence for small κ.

Bremsstrahlung moved positrons from higher to lower energies and therefore also always produced asymmetries larger than the true Δ^0.

Ionization Straggling

Again for each particular target, the theoretical spectra were folded with an ionization-loss distribution function. The peak of this function was constructed by folding the positron starting-point distribution due to the finite target thickness with the peak of the ionization curve given by Landau. [21]

The term "peak" will be used for the part of the ionization-loss distribution function that is associated with values of the Landau parameter, λ, less than 15. [21] This peak describes the distribution of

energy losses due to distant collisions. The term "tail" will be used for the remaining part of the distribution function ($\lambda \gtrsim 15$) which gives the distribution of the large energy transfers in close collisions.

The probable energy losses, required as input for the Landau-curve calculations were obtained from Sternheimer's theoretical formulas[23] which have been confirmed by Hudson's experimental results.[23]

The effect of the Landau peak was an averaging of the spectra over an energy region equal to the base width of the peak. Thus the Landau peak introduced appreciable distortions into the spectra only at their upper ends, where it overlapped them only partially. The asymmetry at these energies was reduced. For energies $x < 0.75$ at which the Landau peak lay entirely within the spectrum, it caused no appreciable corrections to the asymmetry, since the target thicknesses were such that the spectra had essentially constant slope within the base-width of the peak.

Thus the tail alone could produce distortions at the lower energies. Its effect became particularly pronounced at the lowest energies at which measurements were made, because of the combined effects of low intensity and small negative asymmetry relative to the large positive asymmetry at the upper spectrum end. It was required that the tail (a) join the peak smoothly, (b) approach the Bhabha cross section at large fractional energy transfers, and (c) give the correct average energy loss.

An extension of Landau's peak by a function proportional to the inverse square of the energy loss similar to that used by, for example, Leiss et al[24] was tried, but was found to result in average energy losses that were too high by 15 to 70%. (A similar observation was made by Leiss et al[24] during their range-straggling calculations in carbon.)

A tail that did reproduce the average energy losses very well and satisfied the other two requirements by construction, was the asymptotic form of Landau's curve[21] for large energy losses. The $\Delta^0 - \Delta_L$ values of Table II are based on this tail. Although the fractional energy losses involved in these calculations are large (up to 80% of the initial positron energy), Landau's theory is applicable because its chief condition, the energy independence of the energy-loss probability, is well

satisfied for positrons of initial energy between 5 and 50 Mev.

Spectrometer Resolution

The effect of the finite spectrometer resolution was obtained by folding an isosceles triangle of unit height and full width at half maximum equal to $\Delta p/p = 9.30\%$ for the T outputs and 2.32% for the mixing matrix outputs into the uncorrected spectra. A distortion of the asymmetry is again produced, only near the upper spectrum end.

Uncorrected and resolution-corrected asymmetries were compared at the median energy of the positrons at the instant of decay, $\bar{E}$. (See Appendix C for this calculation.)

Magnetic-Field Effect

The presence of large amounts of iron shielding as well as the gradient of the cyclotron and spectrometer stray fields placed limits on the magnetic-field homogeneity that could be achieved with reasonable efforts over the region of the target-counter sandwich. It was also impractical to maintain the precession field at a value required by Eq. (III.4); however, the fields were held constant by continuous monitoring during the runs.

As a consequence, the spectrum obtained when the precession field was turned on (or the stray fields were cancelled) was not exactly equal to the unpolarized (or polarized) spectrum. The resulting effect on the asymmetry (see Appendix D) is reflected in the $\Delta^0 - \Delta_H$ column of Table II, which shows this correction to be appreciable only for the low-energy carbon-target run at $\theta = 39$ deg.

The last column of Table III shows the corrected asymmetry, which is equal to $\Delta_{meas}/\cos\theta$ plus the sum of all corrections.

Uncertainties in Calculated Corrections

A least-mean-squares fit of the theoretical expression for the asymmetry to the measured net asymmetry determined a best-fitting set of parameters ρ, δ, and $R|\xi|$. In order to test the sensitivity of these parameters to variations of the experimental data, the measured energy scale and the measured asymmetry at energies below and above half the

maximum energy were each varied independently by a few percent. The resulting changes in the best-fitting parameter set are noted in Table IV. In this table, $\Delta\rho$ denotes $(\rho_{normal} - \rho_{changed})/\rho_{normal}$. Table IV will be used below to translate calculated uncertainties in the energy scale and the measured asymmetry into uncertainties in the parameter values.

It will now be shown that the uncertainties inherent in the chosen experimental method are associated with negligible uncertainties in the parameters.

From the spectrometer calibration constants given in Section V, it can be seen that the average energy-scale uncertainty is 0.28%, which leads to the uncertainties in ρ, δ, and $R|\xi|$ listed in Table V.

Two other effects influenced the accuracy with which the energy of the positrons at the instant of μ decay could be reconstructed. One was the uncertainty of the path length of the average positron in the targets and counters which was estimated to be at most 1%, because the mass of the targets and counters was known to a few tenths of one percent, and the path length increase due to multiple scattering[25]--neglected in the energy-loss calculations--was also of that order. The average ionization loss is about 15% of the initial energy for the higher energies for which a good energy resolution is important, thus leading to an energy uncertainty of about 0.15%.

The second effect is due to a deviation of the distribution of muon endings in the targets from uniformity by about 10% over the thickness of the average target used in this experiment, while in the ionization-loss calculations, complete uniformity was assumed. This leads to a 3% uncertainty in the average ionization loss (see Appendix E) or a 0.45% uncertainty in the positron energy.

The total calculated correction is estimated to be known to about 2%. The radiative and bremsstrahlung corrections as well as those for ionization straggling constitute the largest part of the total correction. The radiative and bremsstrahlung corrections are accurate to within the fractional contribution of their neglected next-higher-order terms--say,

1%. The ionization-straggling correction is also believed to be known to better than 1% of the total correction, since it was found that any modification of the Landau curve that could change this correction appreciably would also lead to incorrect average-ionization losses. For instance, calculations of the average energy loss by ionization for positrons in lithium using an extrapolation of Landau's peak with the inverse square of the energy loss gave 2.7 Mev/g cm^{-2}. The asymptotic form of Landau's curve gave the correct value of 1.7 Mev/g cm^{-2}. The corresponding values for $\Delta^0 - \Delta_L$ were -5.7% and -1.0% respectively. Therefore, in the low-(high-) energy region where the corrections to the asymmetry are approximately 0.10 (0.05), the asymmetry is uncertain by 0.002 (0.001). These were the values used in compiling Table V.

The individual parameter uncertainties were added in quadrature when computing the total uncertainty of Table V. The 4-deg spread in θ due to the finite solid angle of the spectrometer will cause only a slight decrease of the effective average muon polarization (by about 1%), and will not effect the values of the three parameters.

VII. ANALYSIS OF RESULTS

Best-fitting Parameters

The best-fitting set of parameters ρ, δ, and $R|\xi|$ was obtained from the corrected asymmetries of Table III by using the method for minimizing a function of several variables described by Nierenberg[26] (for details see Appendix F). The calculations were carried out by an IBM 650 computer.

Table VI summarizes the best-fitting parameter sets for various data combinations together with the associated χ^2 values, the degrees of freedom, d, and the probabilities, P, of observing, on repeating the measurements, larger deviations from the theoretical asymmetries computed from the best-fitting parameter sets than those found during this experiment. The notation used for the data combinations is defined in the Section "Definition of Symbols".

The standard deviations of the parameters of Table VI were computed as indicated in Appendix F taking all correlations fully into account. Estimates of these standard deviations obtained by varying each parameter independently about its minimum were smaller in all cases.

The values of P for $d < 30$ were obtained from standard tables while those for $d \geqslant 30$ were computed by assuming that $\sqrt{2\chi^2}$ is normally distributed with unit standard deviation about a mean of $\sqrt{2d-1}$.

The different data combinations were individually least-squares fitted in order to check for internal consistency. Data combinations 1 and 2 show Runs I and II to be consistent with one another. Because comparison of combination 6 with 15, 12 with 16, and 14 with 17 showed that the inclusion of the measured asymmetries at $\bar{E} = 47.72$ and 42.34 Mev of Run I and at $\bar{E} = 52.09$, 51.99, and 51.69 Mev of Run II makes the relative goodness-of-fit poor, these values they were discarded from the data.

Comparison of combination 2 with 3, 4 with 5, etc. checks the consistency of the T with the β_B outputs, while a comparison of 2 with 4, 3 with 5, etc. tests the consistency of the T with the mixing-matrix outputs. Comparison of combination 6 with 12 shows that $R|\xi|$ is almost completely determined by the asymmetry for $X > 0.5$, while for

the determination of the ρ and δ the asymmetry for $x < 0.5$ also is necessary.

For the final summary, the mixing-matrix outputs were preferred over the T outputs because their energy resolution was better on the average by about a factor of 2.5. The data combination with the best energy resolution, 7, gave $\rho = 0.818 \pm 0.057$, $\delta = 0.743 \pm 0.033$, $|\xi| \geqslant R|\xi| = 0.942 \pm 0.062$, and $P = 93\%$; it is plotted in Fig. 12. Data combination 12, which contained the largest number of events, led to $\rho = 0.774 \pm 0.042$, $\delta = 0.782 \pm 0.031$, $|\xi| \geqslant R|\xi| = 0.848 \pm 0.036$, and $P = 70\%$, and was plotted in Fig. 13.

Since the best-fitting ρ and δ values for both these data combinations agreed within their errors with 0.75, their values in the two-component neutrino theory, the question arose whether a least-squares fit of $R|\xi|$ with ρ and δ constrained to 0.75 would also give a good fit. The results, which are listed in the first row of Table VII, indicate that these constrained one-parameter fits are equally as likely as the corresponding three-parameter fits of Table VI. These one-parameter fits are also shown in Fig. 12 and 13.

In order to cross-check the results of Table VI, polynomials in x of orders between 2 and 8 were fitted to data combinations 7 and 12. A third-order polynomial gave the best fit for both combinations, with $P = 73\%$ (94%) for combination 12 (7). These polynomials yielded $\Delta/\cos\theta = 28.06 \pm 2.82\%$ ($31.19 \pm 5.05\%$) at $x = 0.75$, and $\Delta/\cos\theta = (85.47 \pm 3.72\%)$ ($85.70 \pm 4.38\%$) at $x = 1.0$ for combination 12 (7).* Using these values and the relations following Eq. (4), one obtains $R|\xi| = 0.842 \pm 0.085$ (0.936 ± 0.152) which agrees well with Table VI, and $\rho/\delta = 0.985 \pm 0.056$ (1.09 ± 0.12). This value of $R|\xi|$ is independent of ρ and δ. This determination of $R|\xi|$ and ρ/δ assumes only locality and $|\eta| \ll 1$, and it holds for any degree of lepton conservation.

---

*In the remainder of the paper, all quoted results not enclosed in parentheses shall be based on data combination 12, while those so enclosed shall refer to data combination 7, unless other wise stated.

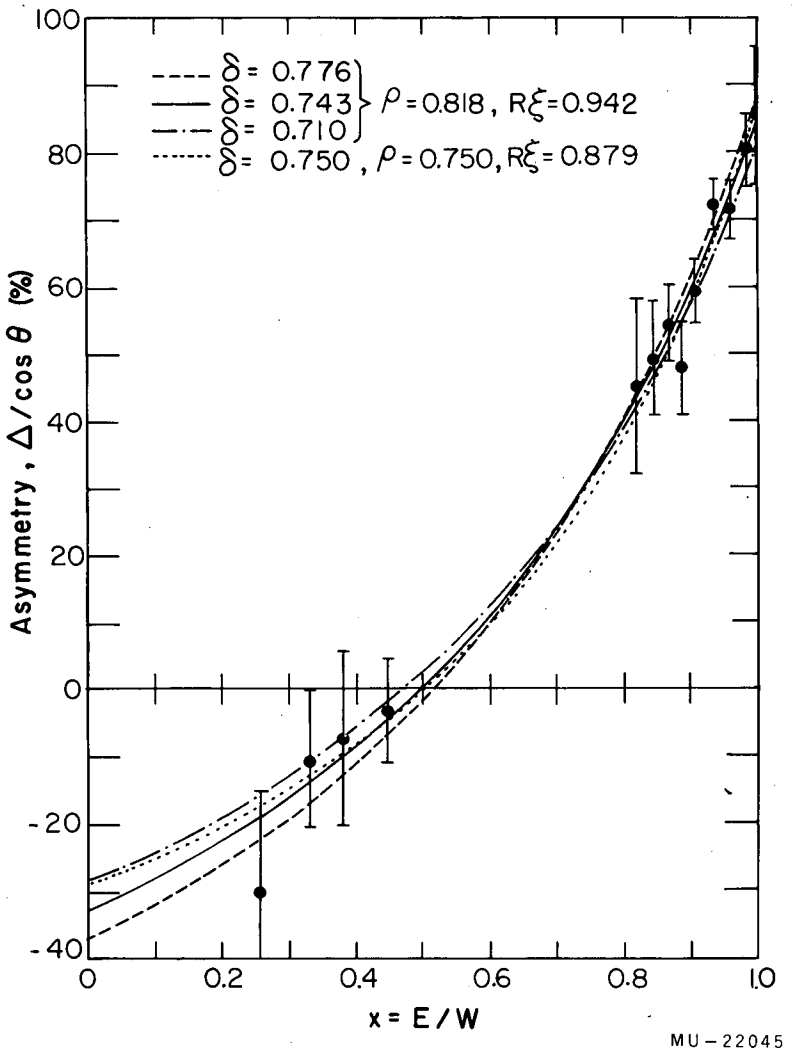

Fig. 12. Data with the best energy resolution, combination 7, and the least-squares-fitted asymmetry curve (solid line). The dashed and dash-dotted lines correspond to a change of δ by one standard deviation from the best fit. The dotted line is the best fit when ρ and δ are restricted to their values in the two-component neutrino theory. The points plotted here and in Fig. 13 are combinations of the data of Table III.

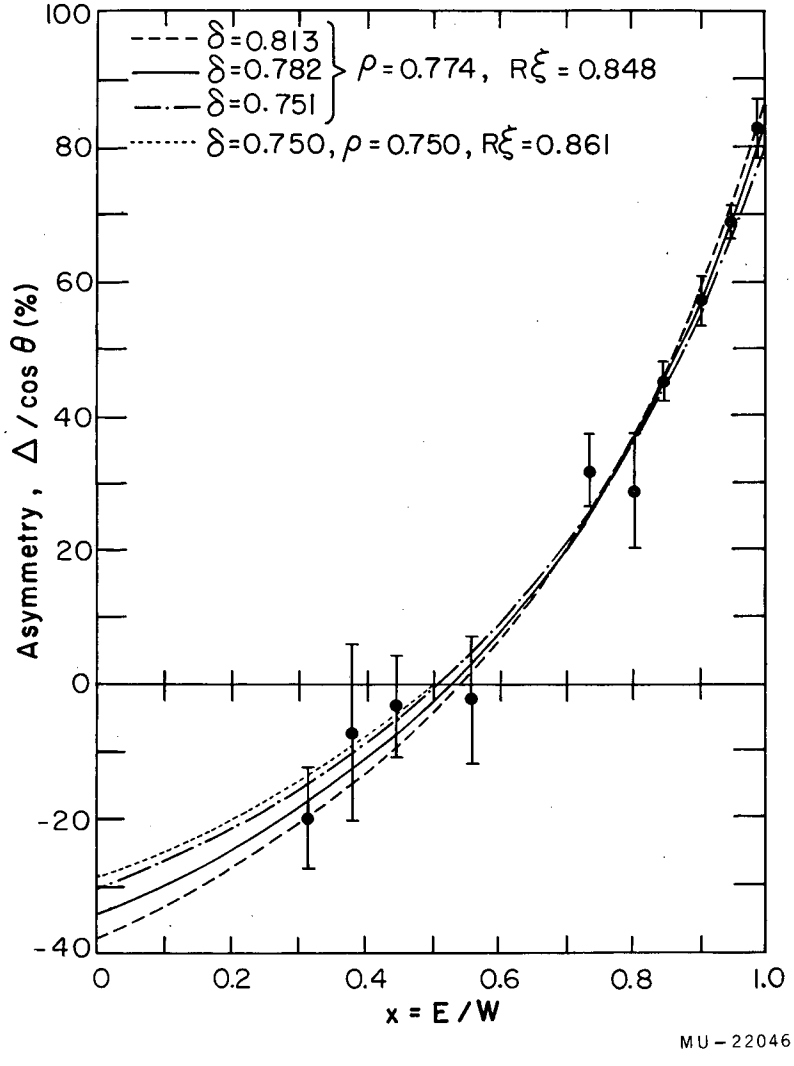

Fig. 13. Total data of this experiment, combination 12, and the least-squares-fitted asymmetry curve (solid line). The dashed and dash-dotted lines correspond to a change of δ by one standard deviation from the best fit. The dotted line is the best fit when ρ and δ are restricted to their values in the two-component neutrino theory. (The dotted line coincides with the dash-dotted one for $0.5 < x < 0.75$ and with the solid one for $x > 0.75$.)

Using Eq. (16) of Appendix G, i.e., $|\xi| = \rho/\delta$, which does not assume lepton conservation or any knowledge of the nature of the μ-decay interaction other than locality, $g_T = -g'_T$, and complete positron polarization, one can compute absolute ξ values from the measured values of ρ and δ. One finds $|\xi| = 0.989 \pm 0.014$ (1.10 ± 0.029) in very good agreement with the ρ/δ values obtained from the third-order polynomial fitted to the asymmetry and evaluated at the points $x = 0.75$ and 1.0.

Taking these $|\xi|$ values and the corresponding values of $R|\xi|$ from Table VI, one may also calculate $R = 0.857 \pm 0.024$ (0.855 ± 0.034).

With these R values, $R|\xi|$ could be held fixed at $R(1.0)$, and one of the parameters ρ or δ could be fitted to the asymmetry while the other was constrained to 0.75 in order to tell whether these values would lie closer to 0.75 than those obtained from the three-parameter fits. The last two rows of Table VII show this to be the case, confirming the compatibility of the data with the (V, A) interaction.

Interpretation

Deviations of experimental μ-decay parameters from their values in the two-component neutrino theory do not necessarily imply the incorrections of the concept of a two-component neutrino. Rather, one can explain these deviations either by admitting a relaxation of the lepton conservation rule or by making the Fermi-type μ-decay interaction nonlocal through the introduction of large-mass intermediary particles propagating between two local Yukawa-type interactions. Relaxation of the lepton conservation rule allows an admixture of μ decay into identical neutrinos with the decay into nonidentical neutrinos (the latter undoubtedly must be the predominent mode, in view of the accumulated experimental evidence about the unpolarized muon spectrum), while maintaining a local Fermi-type interaction. In both cases the two-component picture for the neutrino may be saved.

1. Assumption of Local Interaction with Admixture of μ-Decay into Identical Neutrinos. Using Eq. (20) and (21) of Appendix G and the results in Table VI for combination 12 (or 7), one computes for the

fraction of muons decaying into nonidentical neutrinos 1.032±0.056 (1.091±0.076) from ρ and 1.014±0.013 (0.997±0.015) from δ. Averaging the values obtained from ρ and δ gives 1.023±0.035 (1.044±0.045) or -0.023±0.035 (-0.044±0.045) for the fraction of muons decaying into identical neutrinos. Thus the admixture is not more than about 4% (5%).

2. Assumption of Nonlocal Interaction. First, the question arises whether in a nonlocal theory the radiative corrections to the μ-decay spectra would differ appreciably from those applied to the data presented here which were based on the assumption of a local interaction. Byers and Peierls considered this problem and concluded that the radiative corrections would not be essentially different in a nonlocal theory involving a charged spin-one boson.[27] Thus the results of this experiment may be used to infer characteristics that such a nonlocal interaction needed to be compatible with the data. The theory of a nonlocal muon interaction was first worked out by Lee and Yang,[28] then in greater generality by Bludman and Klein,[29] Sirlin,[30] and Taketani et al.[31]

Bludman distinguishes two kinds of nonlocal interactions. In the first kind, virtual bosons or pairs of fermions connect local momentum independent Yukawa-type interactions (the spectrum is quadratic in positron momentum aside from the phase-space factor). The second kind of interactions are those that owe their nonlocality to the derivative coupling of the positron and neutrino fields (the associated spectrum can be linear, quadratic, or cubic aside from phase space).

The distance over which the nonlocality extends, L, is given by $(\hbar c/M_\mu c^2)l$ or about 2l (using units of 10^{-13} cm). For nonlocal interactions of the first kind, using the second Lagrangian of Lee and Yang[29] i.e. an interaction between charged currents in accordance with the charged nature of the intermediary particle, l in terms of ρ is

$$l^2 = 3\left(\rho - \frac{3}{4}\right).$$

For the second kind, if one assumes the (V-A) interaction for which the spectrum is linear, we have

$$l = \frac{1}{2}(\rho - \delta).$$

The mass of the intermediary particle can be estimated from L, by use of the uncertainty principle, as $M \sim (200/L)$ Mev. Using the values for ρ and δ of data combination 12, one calculates for the first kind of nonlocality $L \cong (0.54 \pm 0.90) \times 10^{-13}$ cm with $M \gtrsim 220$ Mev from ρ. For the second kind, we have $L \cong (-0.008 \pm 0.011) \times 10^{-13}$ cm with $M \gtrsim 20$ Bev from ρ and δ.

There also exist relations between 1 and ξ. However, the values of ξ obtained in this experiment from the ratio of ρ and δ and from the ratio of the asymmetries at $x = 0.75$ and $x = 1.0$ may not be used, since Eq. (16) of Appendix G need not necessarily hold in a nonlocal theory.

A choice between the different kinds of nonlocal interactions can only be made once it has been experimentally determined whether the μ spectrum deviates from linearity.

It is interesting to note that the signs of the deviations of ρ from 3/4 produced by a nonlocality or an admixture of μ decay into identical neutrinos are opposite. Theorists disagree about the expected effect of a nonlocality on ξ,[31, 32] while this effect on δ has apparently not yet been discussed.

Summary

The results of this experiment and their implications are:

(a) Parameters from the fit of the entire asymmetry curve for an unrestricted local interaction are $\rho = 0.774 \pm 0.042$, $\delta = 0.782 \pm 0.031$, and $|\xi| \geqslant R|\xi| = 0.848 \pm 0.036$.

(b) When the μ-decay interaction is restricted to locality, $g_T = -g_T'$, and complete positron polarization, ρ and δ imply $|\xi| = 0.989 \pm 0.014$. Thus the average muon-beam polarization was $R = 0.857 \pm 0.024$ under these conditions.

(c) From the ratio of the points at $x = 0.75$ and 1.0 on the measured asymmetry curve, the ratio ρ/δ for an unrestricted local interaction was found to be 0.985 ± 0.056. This was shown to be the value of $|\xi|$ under the conditions of (b). (The sign of ξ cannot be obtained from this experiment, since it does not measure the helicity of the muon.)

(d) The measured values of ρ, δ, and $|\xi|$ agree within their errors very well with the predictions of the two-component neutrino theory. The data is equally well fitted with the exact values of the two-component neutrino theory with complete positron polarization and with complete lepton conservation, i.e. the V-A interaction for which $\rho = 0.75$, $\delta = 0.75$, and $\xi = -1.0$, if one takes $R = 0.861$. Since in the V, A interaction we have $|\eta| \leq \frac{1}{2}\sqrt{1 - \xi^2}$, the measured value of $R|\xi|$ given in (a) implies $|\eta| \leq 0.27 \pm 0.03$.

(e) The smallness of the deviations of the three parameters from their values in the local two-component neutrino theory with lepton conservation places an upper limit of about 4% on a possible violation of the lepton-conservation rule or restricts the radius of a possible nonlocal interaction propagated by intermediary particles to $(0.54 \pm 0.90) \times 10^{-13}$ cm, and the mass of these particles to $\gtrsim 220$ Mev.

It should be remembered that this experiment does not, of course, prove the two-component nature of the neutrino, but only shows the compatibility of the data with the two-component neutrino theory. Also it does not prove that the μ-decay interaction is V and A only, or that the two decay neutrinos are nonidentical, since one can obtain $\rho = \delta = 3/4$ and $\xi = -1$ if one requires that the muon decay into identical four-component neutrinos and that g_s equals g_p' and g_s' equals g_p, while g_A and g_V' are arbitrary (g_A', g_V, g_T, and g_T' are identically zero for μ decay into identical neutrinos). Only if the two-component neutrino is assumed (for which a μ decay into identical neutrinos demands $\rho = \delta = 0$ and $\xi = -3$) do the measured parameter values prove that most or all of the decay neutrinos are nonidentical.

The results of this experiment are in excellent agreement with those of Plano,[8] who found $\rho = 0.780 \pm 0.025$, $\delta = 0.78 \pm 0.05$, and $R|\xi| = 0.94 \pm 0.07$.

VIII. ACKNOWLEDGMENTS

Without Professor Kenneth M. Crowe's patient guidance, energetic assistance, and most active participation, this experiment could never have been done. I should like to thank him particularly.

I am very grateful for the assistance and advice which I received from Drs. A. Abashian, R. Haddock, P. Macq, and R. Sard during the course of this experiment. Mr. J. Whitsell assumed a large share of the numerical work.

Among the many persons who contributed to the completion of this experiment, I should like to thank especially P. Beilin, G. Bingham, B. Czirr, L. Jellin, C. Keys, T. Maung, H. Pollak, and J. Ryan. J. Vale and L. Houser were in charge of the 184-in. synchrocyclotron operation. I should like to thank Mrs. Virginia Richardson for her enthusiastic efforts in programming the IBM 650 computer.

- - - - - - -

This work was performed under the auspices of the U. S. Atomic Energy Commission.

IX. APPENDICES

A. Propagation of Background Errors

The independently measured quantities are as follows. With targets in, $N_{\downarrow}$ is the number of counts with the precession field turned on, and N_0 is the number of counts with zero field. With the targets out (background) $B_{\downarrow}$ is the number of counts with the precession field turned on, and B_0 is the number of counts with zero field.
Let $M_{\downarrow}$, M_0, $L_{\downarrow}$, and L_0 be the monitor intervals [(μ_1 μ_2) counts] to which all counts are normalized for $N_{\downarrow}$, N_0, $B_{\downarrow}$, and B_0, respectively. Let

$$n_{0'\downarrow} = \frac{N_{0'\downarrow}}{M_{0,\downarrow}}$$

and

$$b = \frac{B}{L} = \frac{B_{\downarrow} + B_0}{L_{\downarrow} + L_0} .$$

Background Assumed Isotropic

If the background is assumed to be isotropic, the asymmetry is

$$\Delta = \frac{n_{\downarrow} - n_0}{n - b} ,$$

and the standard deviation of Δ is

$$s = \left[\left(\frac{\partial \Delta}{\partial N_{\downarrow}} \right)^2 s_{\downarrow}^2 + \left(\frac{\partial \Delta}{\partial N_0} \right)^2 s_0^2 + \left(\frac{\partial}{\partial B} \right)^2 e_B^2 \right] 1/2 ,$$

where

$$s_{\downarrow}^2 = N_{\downarrow} ,$$

$$s_0^2 = N_0 ,$$

$$e_B^2 = B ,$$

$$\frac{\partial \Delta}{\partial N_{\downarrow}} = \frac{1}{M_{\downarrow}} \left[\frac{1}{n_{\downarrow} - b} - \frac{n_{\downarrow} - n_0}{(n_{\downarrow} - b)^2} \right] ,$$

$$\frac{\partial \Delta}{\partial N_0} = - \frac{1}{M_0} \left[\frac{1}{n_{\downarrow} - b} \right],$$

and

$$\frac{\partial \Delta}{\partial B} = \frac{1}{L} \left[\frac{n_{\downarrow} - n_0}{(n_{\downarrow} - b)^2} \right],$$

No Assumptions made about the Nature of the Background

If no assumption are made about the nature of the background, the asymmetry is given by

$$\Delta = 1 - \frac{n_0 - b_0}{n_{\downarrow} - b_{\downarrow}}.$$

The standard deviation of Δ is

$$S = \left[\left(\frac{\partial \Delta}{\partial N_{\downarrow}} \right)^2 S_{\downarrow}^2 + \left(\frac{\partial \Delta}{\partial N_0} \right) S_0^2 + \left(\frac{\partial \Delta}{\partial B_{\downarrow}} \right)^2 e_{\downarrow}^2 + \left(\frac{\partial \Delta}{\partial B_0} \right)^2 e_0^2 \right]^{1/2},$$

where

$$S_{\downarrow}^2 = N_{\downarrow},$$
$$S_0^2 = N_0,$$
$$e_{\downarrow}^2 = B_{\downarrow},$$
$$e_0^2 = B_0,$$

$$\frac{\partial \Delta}{\partial N_{\downarrow}} = \frac{1}{M_{\downarrow}} \left[\frac{n_0 - b_0}{(n_{\downarrow} - b_{\downarrow})^2} \right],$$

$$\frac{\partial \Delta}{\partial N_0} = - \frac{1}{M_0} \left[\frac{1}{n_{\downarrow} - b_{\downarrow}} \right],$$

$$\frac{\partial \Delta}{\partial B_{\downarrow}} = \frac{1}{L_{\downarrow}} \left[\frac{n_0 - b_0}{(n_{\downarrow} - b_{\downarrow})^2} \right],$$

and

$$\frac{\partial \Delta}{\partial B_0} = \frac{1}{L_0} \left[\frac{1}{n_{\downarrow} - b_{\downarrow}} \right].$$

The latter method of background correction was used except for the relatively few cases for which the background had been measured with only one value of the precession field. In these cases, one had to assume an isotropic background.

B. Effect of Muon Stopping Distribution on Background Correction

The wanted quantity is the true asymmetry

$$\Delta^t = 1 - \frac{n_0 - b_0^t}{n_{\downarrow} - b_{\downarrow}^t},$$

where $b_{0,\downarrow}^t$ are the true background rates contributing to the total rates $n_{0,\downarrow}$ when the targets are inserted.

When the targets are removed, the target-dividing counters move to a different position on the muon range curve, the muon stopping rate changes because the range curve is not flat, and one now measures $b_{0,\downarrow} = (1+k)\, b_{0,\downarrow}^t$. Here $b_{0,\downarrow}$ denotes the quantities entered into Table I.

The corresponding asymmetry is

$$\Delta = 1 - \frac{n_0 - b_0}{n_{\downarrow} - b_{\downarrow}} = 1 - \frac{n_0 - (1+k) b_0^t}{n_{\downarrow} - (1+k) b_{\downarrow}^t}.$$

Expanding and neglecting all terms in powers of k higher than the first, we have

$$\Delta = \Delta^t \left[1 + k \frac{b_{\downarrow}^t}{n_{\downarrow} - b_{\downarrow}^t} \right] - k \left[\frac{b_{\downarrow}^t - b_0^t}{n_{\downarrow} - b_{\downarrow}^t} \right]$$

$$\Delta - \Delta^t = k \left[\frac{b_0^t - (1-\Delta^t) b_{\downarrow}^t}{n_{\downarrow} - b_{\downarrow}^t} \right] = k \left[r - (1-\Delta^t) \right] \frac{b_{\downarrow}^t}{n_{\downarrow} - b_{\downarrow}^t},$$

where

$$r \equiv \frac{b_0^t}{b_{\downarrow}^t}.$$

Since we have $r \cong 1$ in almost all cases, we can write

$$\Delta - \Delta^t = k \Delta^t \left(\frac{b^t \downarrow}{n \downarrow - b^t \downarrow} \right).$$

Note that Δ^t is the true measured asymmetry corrected only for background, but not yet corrected for other instrumental effects.

C. Median Positron Energy

When the momentum band of the spectrometer does not completely overlap the positron spectrum, the uncorrected and resolution-corrected asymmetries must be compared at an energy $\overline{E} = \overline{E}_s + \epsilon_{ave}$ such tat $\overline{E}_s$ divides the area of the resolution triangle (which overlaps the spectrum) into two equal parts (see diagram below).

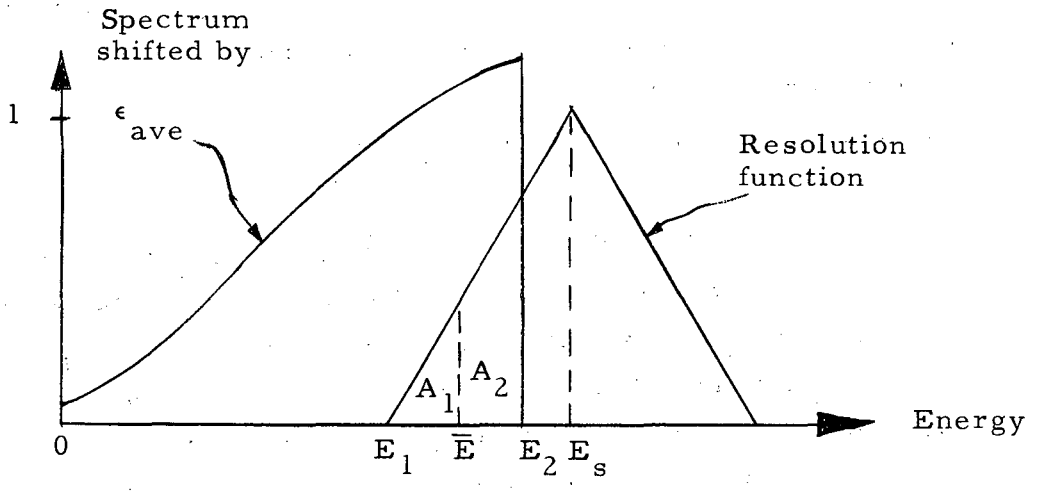

From the condition $A_1 = A_2$ one obtains

$$\bar{E}_s = E_1 + \frac{1}{\sqrt{2}}(E_2 - E_1)$$

for $E_s \geq E_2$, and

$$\bar{E}_s = E_1 + \frac{1}{\sqrt{2}} \left[(E_s - E_1)^2 + (E_s - E_2)^2 \right]^{1/2}$$

for $E_s < E_2$.

Here E_s is the total energy of positrons in the spectrometer, and we define

$$E_2 = W - \epsilon_{ave} = 52.86 \text{ Mev} - \epsilon_{ave},$$

$$E_1 = (1 - \Delta p/p)\ E_s,$$

where ϵ_{ave} is the average energy lost by the positron through ionization as it traverses all material between the point of muon decay and the spectrometer entrance aperture. When the momentum band overlaps the spectrum completely, we have $\bar{E}_s = E_s$.

D. Calculation of Magnetic-Field Effect

Denote by H_0 the magnetic field that existed at the location of the target-counter sandwich when the stray fields were almost cancelled, and by $H_\downarrow$ the field that existed when the precession coil was turned on. Both field were directed downward. Among the different target positions H_0 varied between about 0 and 0.7 gauss, and $H_\downarrow$ between about 56 and 62 gauss.

The corresponding precession angular frequencies are given by

$$\omega_{0,\downarrow} = g_\mu \left(\frac{e\hbar}{2M_\mu c} \right) H_{0,\downarrow}$$

$$\omega_{0,\downarrow} = (8.51 \times 10^4)\ H_{0,\downarrow} \text{ (radians/sec)},$$

where we have $g_\mu = 2.002$, and H is in units of gauss.

Let $N_{0,\downarrow}$ denote the spectra observed when fields $H_{0,\downarrow}$ were turned on. Then from Eq. (6), we have

$$N_{0,\downarrow} = 2x^2 \left\{ G_1 - R\xi \cos\theta \; G_2 F_{0,\downarrow} \right\}; \; F_{0,\downarrow} = F(\omega_{0,\downarrow}).$$

Thus the measured asymmetry is

$$\Delta_H = \frac{N_\downarrow - N_0}{N_\downarrow} = - \Delta \left[\frac{F_\downarrow - F_0}{1 - \Delta F_\downarrow} \right],$$

where Δ is the theoretical asymmetry given by Eq. (4). The (V-A) form of Δ was assumed for the calculation of the correction $\Delta^0 - \Delta_H$.

E. Calculation of Median Target Thickness for Nonuniform Distribution of Muon Endings

For a uniform distribution of muon endings, the median target thickness, $\bar{t}$, is

$$\bar{t} = 1/2 \; t.$$

For a nonuniform distribution of muon endings as illustrated below

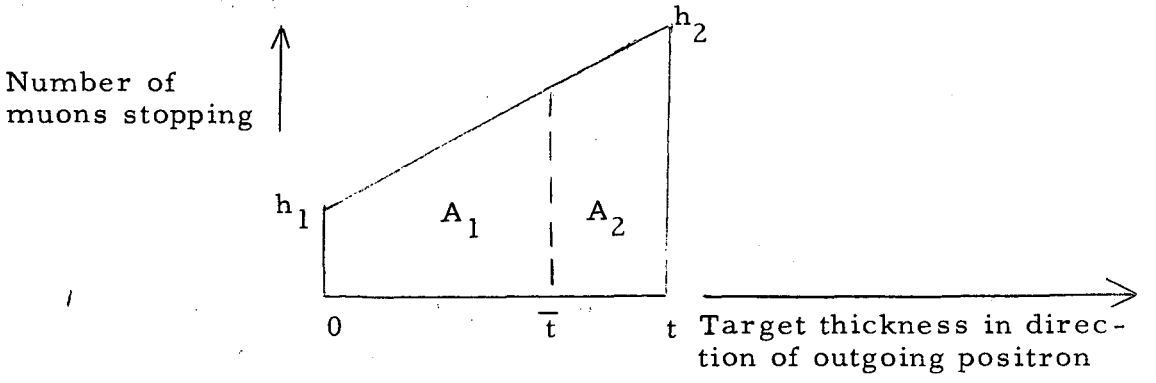

$\bar{t}$ is determined by the condition

$$A_1 = A_2,$$

where

$$A_1 = h_1 \bar{t} + \frac{1}{2}\bar{t}\left(\frac{\bar{t}}{t}\right)(h_2 - h_1)$$

and

$$A_2 = h_2(t-\bar{t}) - \frac{1}{2}(t-\bar{t})\left[(h_2-h_1) - \left(\frac{\bar{t}}{t}\right)(h_2-h_1)\right],$$

or, for $h_1 \neq h_2$,

$$\frac{\bar{t}}{t} = \frac{h_1}{h_1-h_2} - \frac{\sqrt{h_1^2+h_2^2}}{\sqrt{2}\,(h_1-h_2)}.$$

F. Chi-Squared Fit of Spectrum Parameters to Asymmetry

One wants to minimize

$$\chi^2 \equiv \sum_n \left\{ \frac{1}{\epsilon^2} \left[\left(\frac{\Delta}{\cos\theta}\right)_{\text{theoretical}} - \left(\frac{\Delta}{\cos\theta}\right)_{\text{measured}} \right]^2 \right\}_n$$

$= f(\rho, \delta, R\xi)$, where ϵ is the standard deviation associated with the measured $\Delta/\cos\theta$ and the summation extends over all data points.

The condition that f be a minimum for the parameter set $p = (\rho, \delta, R\xi)$ is

$$\sum_i \frac{\partial}{\partial p_i} f = 0$$

where $p_i = \rho, \delta,$ or $R\xi$.

For any set p^0 in the neighborhood of p, one may expand in a Taylor's series about p^0 to get the derivative at p:

$$\left[\sum_i \frac{\partial}{\partial p_i} f\right]_p = \left[\sum_i \frac{\partial}{\partial p_i} f\right]_{p^0} + \left[\sum_{i,j} \frac{\partial^2}{\partial p_i \partial p_j} f\right]_{p^0} dp_j + \ldots = 0,$$

where $dp_j = p_j - p_j^0$.

If the neglected higher derivatives vanish identically, the parameter set that minimizes f, p_j, can be found in one step:

$$p_j = p^0{}_j + dp_j,$$

where p_j^0 is the first trial set and dp_j are the solutions of the three simultaneous linear equations

$$\left[\sum_{i,j} \frac{\partial^2}{\partial p_i \partial p_j} f\right]_{p^0} dp_j = -\left[\sum_i \frac{\partial}{\partial p_i} f\right]_{p^0}.$$

The standard deviation of the jth parameter about its minimum is given by[32]

$$\epsilon_j = \pm \left(1/2\,[D^{-1}]_{jj}\right)^{1/2}, \text{ where } D^{-1} \text{ is the inverse of}$$

the matrix $\frac{\partial^2 f}{\partial p_i \partial p_j}$ evaluated at the minimum.

Where the higher derivatives are not zero, the minimum will in general not be reached in one step, and the calculations must be repeated, always using the p_j of one step as the p_j^0 of the following one.

It was found that there were regions on the hypersurface f where the slope changed so rapidly that f increased in going from p_j^0 to p_j. In this case, convergence was insured by dividing dp_j by powers of two until $f(p_j^0 + 2^{-m}\, dp_j)$ was less than $f(p_j^0)$ $(m = 1, 2, 3, \ldots)$ before proceeding to the next iteration.

G. Effect of an Admixture of μ Decay into Identical Neutrinos on the Spectrum Parameters

Discard for the moment the lepton-conservation rule and admit the reactions $\mu^+ \rightarrow e^+ + 2\nu$ and $\mu^+ \rightarrow e^+ + 2\bar{\nu}$ in addition to $\mu^+ \rightarrow e^+ + \nu + \bar{\nu}$. Let $N_{n,i}$ be the positron spectrum from μ^+ decay into nonidentical or identical neutrinos, respectively, $C_{n,i}$ be the probability that a μ^+ will decay into nonidentical or identical neutrinos, respectively, and $\rho_{n,i}$, $\delta_{n,i}$, and $\xi_{n,i}$ be the parameters of the spectrum for the decay of the μ into nonidentical

or identical neutrinos.

We have

$$N \equiv C_n N_n + C_i N_i \tag{9}$$

with

$$C_n + C_i = 1, \tag{10}$$

where C_n and C_i are real and positive.

The nonidentical-neutrino and identical-neutrino spectra have the same form (see Eq. (1)

$$N_{n,i} \equiv \frac{dN_{n,i}}{dx d(\frac{\Omega}{4\pi})} = 4x^2 \left\{ 3(1-x) + 2\rho_{n,i}(\frac{4}{3}x-1) - R\xi_{n,i}\cos\theta \left[1-x+2\delta_{n,i}(\frac{4}{3}x-1) \right] \right\}. \tag{11}$$

This spectrum is normalized to unity.

The n-neutrino and i-neutrino parameters also have identical forms, which are, for the decay of a positive muon into a right-handed positron,[10]

$$\rho = \frac{3b + 6c}{a+4b+6c},$$

$$\delta = \frac{3b' - 6c'}{-3a'+4b'-14c'},$$

and

$$\xi = \frac{3a'-4b'+14c'}{a+4b+6c},$$

with

$$a = |g_s|^2 + |g_s'|^2 + |g_p|^2 + |g_p'|^2$$

$$b = |g_V|^2 + |g_V'|^2 + |g_A|^2 + |g_A'|^2$$

$$c = |g_T|^2 + |g_T'|^2$$

and

$$a' = 2\,\mathrm{Re}(g_s^* g_p' + g_p^* g_s')$$

$$b' = 2\,\mathrm{Re}(g_V^* g_A' + g_A^* g_V')$$

$$c' = 2\,\mathrm{Re}(g_T^* g_T')$$

General Case: Four Component Neutrinos

If no assumptions are made about the coupling, we have the following relations and conditions:

For the n parameters we have

(a) $0 \leqslant \rho_n \leqslant 1$,

(b) $|\xi_n \delta_n| \leqslant \rho_n$,

(c) $3(3-4\rho_n) + \xi_n(3-4\delta_n) = 0$ (i.e. only two independent parameters)

and

(d) the coupling constants are unrestricted.

For the i parameters we have

(e) $g_V = 0$, $g_A' = 0$, and $g_T = g_T' = 0 \rightarrow c = c' = 0$;

(f) $0 \leqslant \rho_i \leqslant 3/4$;

(g) $\xi_i \delta_i = -\rho_i$;

and

(h) $-\xi_i = 3-8/3\ \rho_i$.

Only one parameter is independent.

When substituting Eq. (11) into Eq. (9), we can obtain a spectrum that is identical in form with the standard spectrum (1) if we use Eq. (10):

$$N = 4x^2\left\{3(1-x) + 2\rho_{eff}(4/3x-1) - R\xi_{eff}\cos\theta\left[1-x+2\delta_{eff}(4/3x-1)\right]\right\}, \tag{12}$$

where we define the effective parameters by

$$\rho_{eff} \equiv C_n \rho_n + C_i \rho_i, \tag{13}$$

$$\delta_{eff} \equiv (C_n \xi_n \delta_n + C_i \xi_i \delta_i)/(C_n \xi_n + C_i \xi_i) \tag{14}$$

and

$$\xi_{eff} = C_n \xi_n + C_i \xi_i. \tag{15}$$

If we assume also that we have 100% positron polarization and $c = |g_T + g_T'|^2 = 0$ (i.e. $g_T = -g_T'$), for the n-neutrino decay then we can write

$$\xi_n \delta_n = -\rho_n,$$

and therefore

$$\xi_{eff}\,\delta_{eff} = -\,\rho_{eff}. \tag{16}$$

Using Eq. (16) and measurements of the ρ and δ parameters for the local Fermi interaction, we can calculate the ξ parameter without knowing the muon polarization regardless of whether leptons are partially or absolutely conserved.

The admixture constant C_i cannot be calculated from the effective parameters in this general case. Further assumptions must be made.

Special Case: Two-Component Neutrinos

If we additionally specializes to the two-component neutrino theory, then we have $\rho_i = \delta_i = 0$, $\xi_i = -3$, and still $\rho_n = \delta_n = 3/4$, $\xi_n = -1$.

Now Eqs. (13), (14), and (15) reduce to[33]

$$\rho_{eff} = 3/4\; C_n, \tag{17}$$

$$\delta_{eff} = \frac{3/4\; C_n}{3\text{-}2\; C_n}, \tag{18}$$

and

$$\xi_{eff} = 2\; C_n - 3. \tag{19}$$

This leads to three redundant equation for C_n

$$C_n = 4/3\; \rho_{eff}, \tag{20}$$

$$C_n = \frac{3\delta_{eff}}{3/4+2\delta_{eff}}, \tag{21}$$

and

$$C_n = 1/2\; (\xi_{eff} + 3). \tag{22}$$

Note that we have $C_i = 1 - C_n$.

One sees that the effect of an admixture of μ decay into identical neutrinos ($C_n < 1$) on the parameters will be $\rho_{eff} < 3/4$, $\delta_{eff} < 3/4$, $|\xi_{eff}| > 1$.

The measured parameters of this experiment may, of course, be identified with the effective parameters of this Appendix.

For the same conditions for which the effective parameters satisfy Eq. (16), they also obey a relation identical to (h). In practice, this relation is not as useful as Eq. (16), because of its relative statistical inefficiency. The same reason renders relation (c) for the n parameters useless in practice.

X. DEFINITION OF SYMBOLS

A. General Notation

θ is the angle between μ^+-spin and positron momentum.

$\bar{E}_s$ is the median spectrometer energy setting (Mev).

t is the average thickness which the positrons traverse from the point of μ^+-decay to the spectrometer entrance aperture.

Δt is the uncertainty in t due to the finite target thickness.

ϵ_{ave} is the average energy loss in traversing t.

$\bar{E}$ is the median positron energy at the instant of decay, which equals $\bar{E}_s + \epsilon_{ave}$.

Δ^0 is Δ for $\theta = 0$ deg, which equals $\Delta/\cos\theta$.

$\Delta\bar{E}$ is the combined uncertainty in $\bar{E}$ due to finite target thickness and finite spectrometer momentum resolution.

Δ' is the asymmetry with radiative corrections included.

Δ_B is the asymmetry with external bremsstrahlung included.

Δ_L is the asymmetry with ionization straggling included.

Δ_S is the asymmetry with spectrometer momentum resolution included.

$N_\downarrow$ is the number of counts with precession field turned on and with targets in.

N_0 is the number of counts with zero field and targets in.

$B_\downarrow$ is the number of counts with precession field turned on and with targets out.

B_0 is the number of counts with zero field and targets out.

$M_\downarrow$ designates the monitor intervals (μ_1 μ_2 coincidences) for $N_\downarrow$.

M_0 designates the monitor intervals for N_0.

$L_\downarrow$ designates monitor intervals for $B_\downarrow$.

L_0 designates monitor intervals for B_0.

The column marked target material shows the nominal thickness of the individual target pieces.

B. Notation Used for Data Combinations

I_T^l designates asymmetry values of Run I for $x < 0.5$ (T outputs).

I_T^h designates asymmetry values of Run I for $x \geq 0.5$ (T outputs).

$I_T^{h'}$ designates asymmetry values of Run I for $x \geq 0.5$ with the measurements at $\bar{E}$ = 47.72 and 42.34 Mev omitted (T outputs).

II_T^l designates asymmetry values for Run II for $x < 0.5$ (T outputs).

II_β^l designates asymmetry values of Run II for $x < 0.5$ (β_B outputs).

II_T^h designates asymmetry values of Run II for $x \geq 0.5$ (T outputs).

$II_T^{h'}$ designates asymmetry values of Run II for $x \geq 0.5$, with the measurements at $\bar{E}$ = 52.09, 51.99, 51.81, and 51.69 Mev omitted (T outputs).

II_M^h designates asymmetry values of Run II for $x \geq 0.5$ (mixing-matrix outputs).

XI. TABLES

Table I. Raw Data

Experiment I

Target material	$\bar{E}$ (Mev)	Targets in				Targets out			
		$M_{\downarrow}$	$N_{\downarrow}$	M_0	N_0	$L_{\downarrow}$	$B_{\downarrow}$	L_0	B_0
1-in. Li	23.23	1,672	285	1,615	251	615	35	460	35
	20.34	1,672	352	1,615	311	615	51	460	40
	17.40	1,672	329	1,615	344	615	33	460	27
2-in. Li	29.11	1,226	373	1,223	309	170	8	258	8
	51.85	612	506	931	535	180	85	227	124
	52.37	200	164	300	208	80	39	130	78
	49.52	186	168	253	119	60	10	-	-
	23.76	1,226	355	1,223	329	170	8	258	10
	47.72	612	846	931	866	180	42	227	59
	49.64	200	240	300	225	80	37	130	32
	44.27	186	339	253	264	60	7	-	-
	18.49	1,226	312	1,223	288	170	13	258	9
	42.34	612	942	931	897	180	32	227	74
	44.30	200	251	300	260	80	9	130	41
	39.91	186	258	253	327	60	11	-	-
0.3-in. $CHBr_3$	51.16	180	96	285	101	60	29	60	29
	47.95	180	128	285	145	60	20	60	29
	42.46	180	269	285	292	60	11	60	12
1-in. C	24.29	82	121	84	118	-	-	40	8
	32.13	242	351	238	356	-	-	16	15
	43.86	241	443	237	347	-	-	32	24
	50.48	390	726	419	487	38	44	-	-
	20.36	12	124	12	112	3	12	-	-
	50.48	8	307	8	472	1.74	5	-	-

Table I. Raw Data (cont'd.)

Experiment II

Target Material	$\bar{E}$ (Mev)	Targets in				Targets out			
		$M_{\downarrow}$	$N_{\downarrow}$	M_0	N_0	$L_{\downarrow}$	$B_{\downarrow}$	L_0	B_0
0.5-in. Li	52.39	104	32	228	61	26	8	117	52
	52.09	211	163	424	142	86	35	158	95
	51.18	284	414	454	300	134	81	219	123
	49.58	132	237	244	237	54.8	42	114	78
	51.99	104	57	228	45	26	8	117	25
	51.69	211	231	424	152	86	19	158	43
	50.07	284	577	454	345	134	45	219	65
	48.85	132	189	244	169	54.8	12	114	30
	51.59	104	101	228	100	26	6	117	18
	50.42	211	297	424	237	86	15	158	44
	49.19	284	606	254	420	134	30	219	57
	47.49	132	256	244	229	54.8	15	114	24
	50.47	104	119	228	115	26	4	117	21
	49.65	211	322	424	265	86	22	158	24
	48.34	284	609	454	421	134	40	219	43
	46.12	132	216	244	196	54.8	10	114	19
	49.47	104	281	228	291	26	14	117	63
	48.83	211	527	424	472	86	47	158	75
	46.97	284	841	454	639	134	67	219	71
	44.76	132	337	244	355	54.8	24	114	55
0.75-in. Li	18.68	1,418	274	1,380	282	247	27	211	22
	16.85	1,418	125	1,380	136	247	4	211	3
	15.00	1,418	206	1,380	201	247	8	211	11
	13.17	1,418	161	1,380	156	247	3	211	7
	11.33	1,418	193	1,380	196	247	21	211	15

Table I. Raw Data (cont'd.)

Experiment II. (cont'd).

Target material	$\bar{E}$ (Mev)	Targets in				Targets out			
		$M_{\downarrow}$	$N_{\downarrow}$	M_0	N_0	$L_{\downarrow}$	$B_{\downarrow}$	L_0	B_0
0.50-in. Li[a]	56.87	2,588	98	5,279	113	910	25	2,347	84
	52.68	1,930	169	3,744	137	742	26	1,655	43
	52.00	2,453	371	4,638	275	991	40	2,029	68
	50.81	2,555	480	4,683	355	1,068	37	2,087	63
	49.39	2,656	564	4,730	415	1,145	31	2,145	75
	48.02	2,190	424	3,868	369	954	26	1,765	49
	46.86	1,724	334	3,006	310	762	37	1,385	39
	46.01	1,097	214	1,884	171	487	8	894	10
	43.72	264	51	488	47	110	3	228	3
	42.38	132	25	244	32	54.8	2	114	3
0.75-in. Li[b]	14.92	1,433	1,853	1,419	1,858	247	107	196	101

[a] Measured with the mixing matrix coincidence circuit.

[b] Measured with the β_B-coincidence circuit.

Table II. Calculated Corrections to Asymmetry

Experiment I									
θ (deg)	Target No.	Target material	$\bar{E}_s$ (Mev)	Calculated corrections (%) $\Delta^0-\Delta^r$	$\Delta^0-\Delta_B$	$\Delta^0-\Delta_L$	$\Delta^0-\Delta_S$	$\Delta^0-\Delta_H$	Total calculated correction (%)
173	1	1-in. Li	15.44	-1.6	-3.9	-3.5	-0.1	-0.1	-9.2
	2		15.44	-1.7	-5.3	-3.3	-0.1	-0.2	-10.6
	3		15.44	-2.0	-2.9	-2.9	-0.1	-0.4	-8.3
	1	2-in. Li	15.44	-0.7	-8.5	-3.7	-0.2	+0.1	-13.0
			37.92	-0.8	-1.9	+7.4	-0.3	+0.1	+4.5
			38.43	-0.3	-1.0	+11.4	+3.6	-0.1	+13.6
			35.75	-0.7	-3.6	+2.9	-0.8	+0.3	-1.9
	2		15.44	-1.5	-6.6	-3.9	-0.1	-0.1	-12.2
			39.18	-0.8	-3.0	0	-0.7	+0.5	-4.0
			41.12	-0.7	-2.5	+0.8	-0.7	+0.4	-2.7
			35.75	-0.9	-3.9	-1.4	-0.5	+0.5	-6.2
	3		15.44	-1.9	-3.8	-2.4	-0.1	-0.3	-8.5
			39.18	-0.3	0	-2.3	-0.4	+0.5	-2.5
			41.12	-0.6	0	-2.4	-0.5	+0.6	-2.9
			35.75	-1.4	-1.5	-2.3	-0.3	+0.4	-5.1
	1	0.3-in.	38.09	-0.5	-4.0	+14.2	-1.1	+0.2	+8.8
	2	$CHBr_3$	39.18	-0.8	-6.5	+7.7	-0.7	+0.5	+0.2
	3		39.18	-1.0	-7.0	-0.6	-0.5	+0.5	-8.6
180	1	1-in. C	19.72	-1.5	-5.6	-2.1	-0.1	-0.2	-9.5
			27.50	-1.3	-4.6	-1.7	-0.2	+0.1	-7.7
			39.18	-1.0	-3.2	-0.8	-0.5	+0.2	-5.3
			45.77	-1.4	-1.7	-1.1	-6.4	+0.2	-10.4
39			15.83	-1.8	-6.3	-2.5	-0.1	+0.1	-10.6
			45.77	-1.4	-1.7	-1.0	-6.4	-9.8	-20.3

Table II. (cont'd)

Experiment II									
θ (deg)	Target No.	Target material	$\bar{E}$ (Mev)	Calculated corrections (%)					Total calculated correction (%)
				$\Delta^0-\Delta'$	$\Delta^0-\Delta_B$	$\Delta^0-\Delta_L$	$\Delta^0-\Delta_S$	$\Delta^0-\Delta_H$	
192	1	0.5-in. Li	45.27	-0.2	-0.3	+8.2	+1.9	-0.4	+9.2
			44.97	-0.4	0	+7.7	+2.0	-0.3	+9.0
			44.06	-0.6	0	+7.2	+0.3	-0.2	+6.7
			42.46	-0.6	-1.7	+6.7	-2.4	+0.1	+2.1
	2		46.24	-0.4	-0.4	+6.3	+1.6	+0.3	+6.8
			45.93	-0.4	-0.6	+5.9	+0.9	-0.3	+5.5
			44.31	-0.7	-1.2	+4.0	-2.5	-0.1	-0.5
			43.10	-2.2	-1.7	+1.3	-0.6	0	-3.2
	3		47.20	-0.3	-0.5	+4.5	+1.6	-0.6	+4.7
			46.04	-0.6	-0.9	+3.6	-3.4	-0.5	-1.8
			44.81	-0.7	-1.2	+2.8	-2.4	-0.4	-1.9
			43.10	-2.1	-1.6	-0.4	-0.7	0	-4.8
	4		47.44	-1.0	0	+1.8	-2.4	-0.4	-2.0
			46.63	-1.1	-0.4	+1.1	-3.4	+0.3	-4.1
			45.31	-0.6	-1.0	+0.9	-0.7	+0.1	-1.5
			43.10	-0.8	-1.3	0	-0.7	+0.1	-2.7
	5		47.81	-0.6	-0.5	+0.4	-3.7	-0.4	-4.7
			47.17	-0.7	-0.6	+0.1	-2.3	-0.3	-3.8
			45.31	-0.7	-0.8	+0.3	-0.4	-0.1	-1.7
			43.10	-0.9	-1.0	-0.3	-0.6	+0.1	-2.6

Table II. (cont'd)

Experiment II									
θ (deg)	Target No.	Target material	$\bar{E}$ (Mev)	Calculated corrections (%)					Total calculated correction (%)
				$\Delta^0-\Delta'$	$\Delta^0-\Delta_B$	$\Delta^0-\Delta_L$	$\Delta^0-\Delta_S$	$\Delta^0-\Delta_H$	
39	1	0.75-in. Li	9.83	-1.8	-8.1	-2.7	-0.1	+0.6	-12.1
	2		9.83	-2.0	-7.5	-2.6	-0.1	+0.6	-11.6
	3		9.83	-2.3	-6.7	-2.2	-0.1	+0.3	-11.0
	4		9.83	-2.6	-5.5	-2.7	-0.1	+0.1	-10.8
	5		9.83	-3.2	-3.6	-1.0	-0.1	+0.5	- 7.4

Table III. Corrected asymmetry

Experiment I									
θ (deg)	Target No.	$\bar{E}_s$ (Mev)	$t \pm \Delta t$ (g/cm^2)	Target material	$\bar{E} \pm \Delta \bar{E}$ (Mev)	Uncorrected asymmetry $\Delta_{meas.}/\cos\theta$ (%)	Background-corrected asymmetry $\Delta_{meas.}/\cos\theta$ (%)	Total calculated corrections (%)	Net asymmetry $\Delta/\cos\theta$ (%)
173	1	15.44	5.22±0.68	1-in. Li	23.24±2.49	+8.9±8.0	+14.4±16.3	-9.2	+5.2±16.3
	2	15.44	3.42±0.68		20.34±2.49	+8.6±7.9	+17.4±17.4	-10.6	+6.8±17.4
	3	15.44	1.63±0.68		17.40±2.49	-8.3±7.8	- 7.9±15.7	-8.3	-16.2±15.7
	1	15.44	8.61±1.36	2-in. Li	29.11±3.61	+17.1±6.4	+14.0±10.5	-13.0	+1.0±10.5
		37.92			51.85±5.66	+30.7±4.2	+92.4±16.1	+4.5	+96.9±16.1
		38.43			52.37±5.78	+15.6±8.9	+72.6±26.6	+13.6	+86.2±26.6
		35.75			49.52±5.44	+48.4±6.2	+59.2± 8.3	-1.9	+57.3± 8.3
	2	15.44	5.46±1.36		23.76±3.61	+7.2±7.7	+ 5.2±12.0	+12.2	-7.0±12.0
		39.18			47.72±5.75	+32.9±3.2	+41.9± 5.1	-4.0	+37.9± 5.1
		41.12			49.64±5.92	+37.7±5.8	+47.5±13.6	-2.7	+44.8±13.6
		35.75			44.27±5.44	+43.0±4.7	+46.2± 5.1	-6.2	+40.0± 5.1
	3	15.44	2.31±1.36		18.49±3.61	+7.5±7.6	-12.7±18.9	-8.5	-21.2±18.9
		39.18			42.34±5.75	+37.7±2.9	+53.6± 4.2	-2.5	+51.1± 4.2
		41.12			44.30±5.92	+31.4±6.1	+51.6± 7.4	-2.9	+48.7± 7.4
		35.75			38.91±5.44	+33.1±5.1	+36.9± 5.6	-5.1	+31.8± 5.6
	1	38.09	7.55±1.10	0.3-in. $CHBr_3$	51.16±5.16	+33.9±9.6	+360.7±508.8	+8.8	+369.5±508.8
	2	39.18	7.55±1.10		47.95±5.22	+28.8±8.8	+93.8±20.6	+0.2	+94.0±20.6

Table III. Corrected asymmetry (cont'd.)

θ (deg)	Target No.	$\bar{E}_s$ (Mev)	$t \pm \Delta t$ (g/cm^2)	Target material	$\bar{E} \pm \Delta \bar{E}$ (Mev)	Uncorrected asymmetry $\Delta_{meas.}/\cos\theta$ (%)	Background-corrected asymmetry $\Delta_{meas.}/\cos\theta$ (%)	Total calculated corrections (%)	Net asymmetry $\Delta/\cos\theta$ (%)
	3	39.18	4.86±1.10	0.3-in. $CHBr_3$	42.46±5.22	+31.3±5.8	+37.4±9.0	-8.6	+28.8±9.0
180	1	19.72	2.47±2.03	1-in. C	24.29±5.53	+ 2.5±12.3	+ 5.5±26.8	-9.5	4.0±12.3
		27.50			32.13±6.23	- 2.9± 5.5	- 8.2±22.9	-7.7	-15.9±22.9
		39.18			43.86±7.29	+20.0± 5.7	+34.9± 8.9	-5.3	+29.6± 8.9
		45.77			50.48±7.93	+37.4± 3.7	+70.7±11.5	-10.4	+60.3±11.5
39		15.83			20.36±5.18	-12.5±15.2	-23.4±24.1	-10.6	-34.0±24.1
		45.77			50.48±7.93	+69.1±14.5	+74.8±16.2	-20.3	+54.5±16.2
					Experiment II				
192	1	45.27	4.17±0.34	0.50-in. Li	52.39±4.77	+13.3±19.3		+9.2	---
		44.97			52.09±4.74	+58.0± 5.1	+130.5±26.4	+9.0	+139.5±26.4
		44.06			51.18±4.66	+55.8± 3.5	+ 90.4± 5.7	+6.7	+ 97.1± 5.7
		42.46			49.58±4.51	+46.8± 5.1	+ 73.7±10.9	+2.1	+ 75.8±10.9
	2	46.24	3.37±0.34		51.99±4.86	+65.4± 7.4	+109.2±14.3	+6.8	+116.0±14.3
		45.93			51.69±4.83	+68.8± 3.5	+ 92.2± 6.0	+5.5	+ 97.7± 6.0
		44.31			50.07±4.68	+64.0± 2.7	+ 74.4±12.1	-0.5	+ 73.9±12.1
		43.10			48.85±4.56	+52.7± 5.2	+ 66.0± 7.0	-3.2	+ 62.8± 7.0

Table III. (cont'd.) Experiment II

θ (deg)	Target No.	$\bar{E}_s$ (Mev)	$t \pm \Delta t$ (g/cm^2)	Target material	$\bar{E} \pm \Delta \bar{E}$ (Mev)	Uncorrected asymmetry $\Delta_{meas.}/\cos\theta$ (%)	Background-corrected asymmetry $\Delta_{meas.}/\cos\theta$ (%)	Total calculated corrections (%)	Net asymmetry $\Delta/\cos\theta$ (%)
192	3	47.20	2.57±0.34	0.50-in.Li	51.59±4.95	+56.0± 6.5	+62.9± 9.5	+4.7	+58.2± 9.5
		46.04			50.42±4.84	+61.5± 3.6	+79.0± 4.8	-1.8	+77.2± 4.8
		44.81			49.19±4.73	+58.2± 2.8	+66.7±11.2	-1.9	+64.8±11.2
		43.10			47.49±4.56	+52.7± 4.5	+57.5± 6.0	-4.8	+52.7± 6.0
	4	47.44	1.78±0.34		50.47±4.97	+57.3± 5.9	+68.7± 7.7	-2.0	+66.7± 7.7
		46.63			49.65±4.90	+60.4± 3.5	+66.4± 7.7	-4.1	+62.3± 7.7
		45.31			48.34±4.77	+57.9± 2.9	+61.9±10.4	-1.5	+60.4±10.4
		43.10			46.12±4.56	+52.0± 4.9	+57.4± 6.2	-2.7	+54.7± 6.2
	5	47.81	0.98±0.34	0.50-in.Li	49.47±5.01	+54.0± 4.1	+67.4± 4.9	-4.7	+62.7± 4.9
		47.17			48.83±4.95	+56.6± 2.9	+68.9± 4.5	-3.8	+65.1± 4.5
		45.31			46.97±4.77	+53.7± 2.6	+57.3±17.2	-1.7	+55.6±17.2
		43.10			44.76±4.56	+43.8± 4.5	+55.2± 6.1	-2.6	+52.6± 6.1
39	1	9.83	5.48±0.51	0.75-in.Li	18.68±1.73	+ 7.1±11.6	+25.0± 58.8	-12.1	+12.9±58.8
	2	9.83	4.34±0.51		16.85±1.73	+15.2±17.9	+22.1± 21.4	-11.6	+10.5±21.4
	3	9.83	3.20±0.51		15.00±1.73	+ 0.1±12.7	-22.0± 25.7	-11.0	-33.0±25.7
	4	9.83	2.07±0.51		13.17±1.73	- 0.6±14.4	-19.9± 18.7	-10.8	-30.7±18.7
	5	9.83	0.93±0.51		11.33±1.73	+ 5.3±13.6	+50.3± 90.3	-7.4	+42.9±90.3

Table III (cont'd.) Experiment II

Target thickness and material	$\bar{E} \pm \Delta \bar{E}$ (Mev)	Uncorrected asymmetry $\Delta_{meas.}/\cos\theta$ (%)	Background-corrected asymmetry $\Delta_{meas.}/\cos\theta$ (%)	Total calculated corrections (%)	Net asymmetry $\Delta/\cos\theta$ (%)
0.50-in. Li[a]	56.87±3.91	+44.4± 8.0	+243.6±100.9	---	+243.9±100.9
	52.68±1.87	+59.5± 4.9	+ 81.6± 10.5	+4.1	+ 85.7± 10.5
	52.00±2.65	+62.2± 3.2	+ 78.5± 5.4	+2.2	+ 80.7± 5.4
	50.81±2.08	+61.0± 2.9	+ 71.8± 4.2	-0.1	+ 71.7± 4.2
	49.39±2.11	+60.0± 2.8	+ 73.1± 3.7	-0.7	+ 72.4± 3.7
	48.02±2.17	+51.8± 3.6	+ 60.6± 4.8	-1.1	+ 59.5± 4.8
	46.86±2.05	+47.9± 4.3	+ 49.5± 7.1	-1.5	+ 48.0± 7.1
	46.01±1.79	+54.7± 4.9	+ 56.7± 5.8	-2.1	+ 54.6± 5.8
	44.71±1.86	+51.4± 5.8	+ 51.3± 8.6	-2.0	+ 49.3± 8.6
	43.72±1.57	+51.2±10.2	+ 50.9± 14.4	-2.1	+ 48.8± 14.4
	42.38±1.54	+31.2± 18.9	+ 32.0± 29.9	-2.1	+ 29.9± 29.9
0.75-in. Li[b]	14.92±5.10	+ 1.8± 4.3	- 9.7± 9.8	-10.8	- 20.5± 9.8

[a] Measured with the mixing-matrix coincidence circuit.

[b] Measured with the β_B coincidence circuit.

Table IV. Sensitivity of parameters to systematic errors

Change of input data	Resultant change in the parameters				
	$\Delta\rho$ (%)	$\Delta\delta$ (%)	$\Delta(R\xi)$ (%)	ΔR (%)	$\Delta\xi$ (%)
Energy scale decreased by 1%	+1.0	+1.0	-4.0	-4.0	0
Asymmetry for $x < 0.5$ decreased by 0.01	-0.7	-1.2	+1.2	0	+0.5
Asymmetry for $x > 0.5$ decreased by 5%	-0.8	-1.3	+5.5	+5.0	+0.5

Table V. Summary of uncertainties in calculated corrections

Source of errors	Estimate of errors	Effect on parameters				
		$\Delta\rho$ (%)	$\Delta\delta$ (%)	$\Delta(R\xi)$ (%)	ΔR (%)	$\Delta\xi$ (%)
Spectrometer calibration	Average energy scale uncertainty 0.28%	0.0021	0.0021	0.0100	0.0100	0
Positron path-length in targets	Positron energy uncertainty 0.15%	0.0011	0.0011	0.0054	0.0054	0
Nonuniformity of muon endings in targets	Positron energy uncertainty 0.45%	0.0033	0.0033	0.0162	0.0162	0
Calculation of asymmetry corrections	Low-energy end: Asymmetry uncertainty 0.002	0.0011	0.0018	0.0009	0	0.0010
	High-energy end; asymmetry uncertainty 0.001	0.0001	0.0002	0.0009	0.0009	0.0001
Total effect on parameters		0.004	0.004	0.020	0.020	0.001

Table VI. Chi-squared fit of parameters

No.	Data combination I_T^l	I_T^h	I_T^h	II_T^l	II_β^l	II_T^h	$II_T^{h'}$	II_M^h	ρ	δ	R|ξ|	χ^2	degrees of freedom	Probability of larger deviation (%)
1	X		X						0.830±0.084	0.763±0.036	0.827±0.050	17.2	18	50
2				X				X	0.809±0.064	0.733±0.059	0.945±0.070	6.82	11	78
3					X			X	0.833±0.058	0.776±0.051	0.918±0.070	4.00	7	76
4				X			X		0.961±0.093	0.690±0.043	1.083±0.095	11.3	16	76
5					X		X		0.975±0.086	0.721±0.042	1.055±0.095	8.60	12	72
6			X					X	0.795±0.082	0.813±0.089	0.836±0.044	21.5	21	43
7	X			X				X	0.818±0.057	0.743±0.033	0.942±0.062	9.44	18	93
8	X				X			X	0.829±0.057	0.756±0.032	0.936±0.063	6.66	14	93
9	X			X			X		0.968±0.085	0.714±0.027	1.058±0.082	13.9	23	92
10	X				X		X		0.978±0.082	0.723±0.027	1.055±0.082	11.1	19	93
11	X		X	X				X	0.761±0.043	0.768±0.033	0.851±0.037	27.1	33	77
12	X		X		X			X	0.774±0.042	0.782±0.031	0.848±0.036	24.3	29	70
13	X		X	X			X		0.824±0.051	0.760±0.030	0.884±0.041	31.6	38	77
14	X		X		X		X		0.837±0.050	0.771±0.028	0.883±0.041	28.8	34	73
15		X						X	0.703±0.110	0.631±0.099	0.937±0.041	47.1	23	0.16
16	X	X			X			X	0.835±0.044	0.750±0.027	0.912±0.033	50.1	31	1.5
17	X	X			X	X			0.634±0.047	0.732±0.038	0.817±0.032	88.0	40	5.8×10^{-4}

Table VII. One-parameter chi-squared fits

Fixed parameter	Data combination 7			Data combination 12		
	p = 22 d = p - 2 = 20			p = 33 d = p - 2 = 31		
	Free parameter	χ^2	Probability of larger deviation (%)	Free parameter	χ^2	Probability of larger deviation (%)
$\rho = 0.750$ $\delta = 0.750$	$R\|\xi\| = 0.879 \pm 0.025$	9.82	96	$R\|\xi\| = 0.861 \pm 0.022$	24.60	79
$\rho = 0.750$ $R\|\xi\| = R(1.0)$	$\delta = 0.771 \pm 0.039$	9.98	96	$\delta = 0.757 \pm 0.031$	24.54	79
$\delta = 0.750$ $R\|\xi\| = R(1.0)$	$\rho = 0.728 \pm 0.050$	10.18	95	$\rho = 0.748 \pm 0.041$	24.62	79

XII. REFERENCES

1. L. Rosenson, Phys. Rev. 109, 958 (1958).
2. W. F. Duziak, R. Sagane, and J. Vedder, Phys. Rev. 114, 336 (1959).
3. K. M. Crowe, R. H. Helm, and G. W. Tautfest, Phys. Rev. 99, 872 (1955).
   K. M. Crowe, Bull. Am. Phys. Soc., Series II 2, 206 (1957).
4. R. L. Garwin, L. M. Lederman, and M. Weinrich, Phys. Rev. 105, 1415 (1957).
5. G. Lynch, J. Orear, and S. Rosendorff, Phys. Rev. Letters 1, 471 (1958) and Phys. Rev. 118, 284 (1960).
6. D. Berley, T. Coffin, R. L. Garwin, L. M. Lederman, and M. Weinrich, Phys. Rev. 106, 835 (1957).
7. H. Kruger and K. M. Crowe, Phys. Rev. 113, 341 (1959).
8. R. J. Plano, Phys. Rev. 119, 1400 (1960).
9. T. Kinoshita and A. Sirlin, Phys. Rev. 106, 1110 (1957).
10. T. Kinoshita and A. Sirlin, Phys. Rev. 108, 844 (1957).
11. L. Michel and R. Stora, Compt. rend. 234, 1257 (1952).
    C. Bouchiat and L. Michel, Phys. Rev. 106, 170 (1957). There is an error in this latter paper: the second quantity in the cosine term should read $2\beta(3W-4E+\epsilon^2E^{-1})$ in the notation of these authors.
12. T. D. Lee and C. N. Yang, Phys. Rev. 105, 1671 (1957).
13. G. Culligan, S.G.F. Frank, J.R. Holt, J. C. Kluyver, and T. Massam, Nature 180, 751 (1957); P. Macq, K. Crowe, and R. Haddock, Phys. Rev. 112, 2061 (1958).
14. Search for Neutrinoless Conversion of Muon into Electron, R. D. Sard, K. M. Crowe, and H. Kruger, Phys. Rev. 121, 619 (1961).
15. First-order theory of the double-focusing spectrometer is discussed in D. L. Judd, Rev. Sci. Instr. 21, 213 (1950). See Judd's bibliography for prior publications dealing with this subject. Second-order theory is discussed in D. L. Judd and S. A. Bludman, Nucl. Inst. 1, 46 (1957).

16. R. A. Swanson, Phys. Rev. 112, 580 (1958).
17. For circuit details see the Radiation Laboratory Counting Handbook, UCRL-3307 Rev., Jan. 1, 1959. The Swift discriminator is discussed in D. F. Swift and V. Perez-Mendez, Rev. Sci. Instr. 30, 865 (1959).
18. T. Kinoshita and A. Sirlin, Phys. Rev. 113, 1652 (1957); S. M. Berman, Phys. Rev. 112, 267 (1958); V. P. Kuznetsov, J. Exptl. Theoret. Phys. (U.S.S.R.) 37, 1102 (1959) [translation: Soviet Phys.-JETP 37 (10), 784 (1960)].
19. J. A. Wheeler and W. E. Lamb, Phys. Rev. 55, 858 (1939) as corrected by these authors in Phys. Rev. 101, 1836 (1956).
20. W. Heitler, The Quantum Theory of Radiation Third edition, (University Press, Oxford, 1954) p. 379, Eq. (17).
21. L. Landau, J. Phys. (U.S.S.R.) 8, 201 (1944).
22. R. M. Sternheimer, Phys. Rev. 103, 511 (1956); for earlier Sternheimer papers see references given here.
23. A. M. Hudson, Phys. Rev. 105, 1 (1957).
24. J. E. Leiss, S. Penner, and C. S. Robinson, Phys. Rev. 107, 1544 (1957).
25. On Small Angle Multiple Scattering in Confined Bodies, Helge Øveras, CERN Report 60-18, Geneva, 1960.
26. William A. Nierenberg, A Method for Minimizing a Function of n Variables, UCRL-3816 Rev., August 1959.
27. N. Byers and R. E. Peierls, Nuovo cimento 10, 520 (1958).
28. T. D. Lee and C. N. Yang, Phys. Rev. 108, 1611 (1957).
29. S. Bludman and A. Klein, Phys. Rev. 109, 550 (1958).
30. A. Sirlin, Phys. Rev. 111, 337 (1958).
31. M. Taketani, Y. Katayma, P. L. Ferreira, G. W. Bund, and P. R. de Paula e Silva, Progr. Theoret. Phys. 21, 799 (1959).
32. Jay Orear, Nots on Statistics for Physicists, UCRL-8417, August 13, 1958.
33. Equation (9) has already been derived by M. H. Friedman directly from the two-component neutrino forms of the identical and nonidentical neutrino spectra, Phys. Rev. 106, 387 (1957).

ADDITIONAL SELECTED REFERENCES

Theory

"Question of Parity Conservation in Weak Interactions," T. D. Lee and C. N. Yang, Phys. Rev. 104, 254 (1956).

"On Parity Conservation and Neutrino Mass," A. Salam, Nuovo cimento 5, 299 (1957).

"On the Conservation Laws for Weak Interactions," L. Landau, Nuclear Phys. 3, 127 (1957).

"Parity Nonconservation and Two-Component Theory of the Neutrino," T. D. Lee and C. N. Yang, Phys. Rev. 105, 1671 (1957).

"Parity Nonconservation and the Theory of the Neutrino," J. A. McLennan, Jr., Phys. Rev. 106, 821 (1957).

"Polarization of Electrons in Muon Decay and the Two-Component Theory of the Neutrino," T. Kinoshita and A. Sirlin, Phys. Rev. 106, 1110 (1957).

"Polarization of Electrons from μ-e Decay," H. Uberall, Nuovo cimento 6, 376 (1957).

"On the Polarization of Electrons from Decay of Muons," L. B. Okun and V. M. Sehter, Nuovo cimento 10, 359 (1958).

"Mu Decay with Non-Conservation of Parity," S. Larsen, E. Lubkin, and M. Tausner, Phys. Rev. 107, 856 (1957).

"Radiative Corrections to Muon Decay," R. J. Finkelstein and R. E. Behrends, Phys. Rev. 97, 568 (1955). [Erratum: Phys. Rev. 98, 1870 (1955).]

"Radiative Corrections to Decay Processes," R. E. Behrends, R. J. Finkelstein, and A. Sirlin, Phys. Rev. 101, 866 (1956).

"Muon Decay with Parity Non-Conserving Interactions and Radiative Corrections in the Two-Component Theory," T. Kinoshita and A. Sirlin, Phys. Rev. 107, 593 (1957). (Also see corrections to this report in reference 19.)

"Radiative Corrections to the Asymmetry Parameter of Low-Energy Positrons in Muon Decay," T. Kinoshita and A. Sirlin, Phys. Rev. 107, 638 (1957).

Measurements of ρ

With Nuclear Emulsions

H. J. Bramson and W. W. Havens, Phys. Rev. 83, 861 (1951)

H. J. Bramson, A. M. Seifert, and W. W. Havens, Phys. Rev. 88, 304 (1952).

A. Bonnetti, R. Levi-Setti, M. Panetti, G. Rossi, and G. Tomasini, Nuovo cimento 3, 33 (1956).

C. Besson and V. Brisson-Fouché, Nuovo cimento 10, 1143 (1958).

With Cloud Chambers

R. B. Leighton, C. D. Anderson, and A. J. Seriff, Phys. Rev. 75, 1466 (1949).

A. Lagarrigue and C. Peyrou, J. Phys. Radium 12, 848 (1951).

H. W. Hubbard, The Positron Spectrum from the Decay of the μ Meson, UCRL-1623, March 10, 1952.

J. A. Vilain and R. W. Williams, Phys. Rev. 94, 1011 (1954).

C. P. Sargent, M. Rinehart, L. M. Lederman, and K. C. Rogers, Phys. Rev. 99, 885 (1955).

Measurements of $R|\xi|$

With Nuclear Emulsions

J. I. Friedman and V. L. Telegdi, Phys. Rev. 106, 1290 (1957).

S. A. Ali-Zade, I. I. Gurevich, U. P. Dobretsov, B. A. Nikol'skii, and L. V. Surkova, J. Exptl. Theoret. Phys. (U.S.S.R.) 36, 1327 (1959) [translation: Soviet Phys. -JETP 36(9), 940 (1959)].

W. H. Barkas, P. C. Giles, H. H. Heckman, F. W. Inman, and F. M. Smith, Phys. Rev. 107, 911 (1957).

C. Castagnoli, C. Franzinetti, and A. Manfredini, Nuovo cimento 5, 684 (1957).

N. N. Biswas, M. Ceccarelli, and J. Crussard, Nuovo cimento 5, 756 (1957).

P. H. Fowler, P. S. Freier, C. M. G. Lattes, E. P. Ney, and S. J. St. Lorant, Nuovo cimento 6, 63 (1957).

B. Bhowmik, D. Evans, and D. J. Prowse, Nuovo cimento 5, 1663 (1957).

G. B. Chadwick, S. A. Durrani, L. M. Eisberg, P. B. Jones, J. W. C. Wignall, and D. H. Wilkinson, Phil. Mag. 2, 684 (1957).

D. F. Davis, A. Engler, C. J. Goebel, T. F. Hoang, M. F. Kaplon, and J. Klarmann, Nuovo cimento 6, 311 (1957).

J. K. Bøggild, K. H. Hansen, and M. Scharff, Nuovo cimento 8, 767 (1958).

I. I. Gurevich, V. M. Kutokova, A. P. Mishakova, B. A. Nikol'skii, and L. V. Surkova, J. Exptl. Theoret. Phys. 34 (7), 195 (1958).

Iu. M. Ivanov and V. G. Kirillov-Ugriumov, J. Exptl. Theoret. Phys. (U.S.S.R.) 34, 255 (1958) [translation: Soviet Phys.-JETP 34 (7), 177 (1958)].

Kh. P. Babaian, N. A. Marutian, K. A. Matevosian, and M. G. Sarinian, J. Exptl. Theoret. Phys. (U.S.S.R.) 35, 561 (1958) [translation: Soviet Phys.-JETP 34(7), 195 (1958)].

A. O. Vaisenberg, V. A. Smirnitskii, E. D. Kolganova, and N. V. Rabin, J. Exptl. Theoret. Phys. (U.S.S.R.) 37, 326 (1959) [translation: Soviet Phys.-JETP 37(10), 231 (1959)].

A. O. Vaisenberg, J. Exptl. Theoret. Phys. (U.S.S.R.) 37, 566 (1959) [translation: 37(10), 401 (1959)].

With Bubble Chamber

A. Abashian, R, K. Adair, R. Cook, A. Erwin, J. Kopp, L. Leipuner, T. W. Morris, D. C. Rahm, R. R. Rau, A. M. Thorndike, W. L. Whittemore, and W. J. Willis, Phys. Rev. 105, 1927 (1957).

I. A. Pless, A. E. Brenner, R. W. Williams, R. Bizzari, R. H. Hildebrand, R. H. Milburn, A. M. Shapiro, K. Strauch, J. C. Street, and L. A. Young, Phys. Rev. 108, 159 (1957).

M. H. Alston, W. H. Evans, T. D. N. Morgan, R. W. Newport, and P. R. Williams, Phil. Mag. 2, 1143 (1957).

V. V. Barmin, V. P. Kanavets, B. V. Morozov, and I. I. Pershin, J. Exptl. Theoret. Phys. (U.S.S.R.) 34, 830 (1958) [translation: Soviet Phys.-JETP 34 (7), 573 (1958)].

A. I. Alikhanian, V. G. Kirillov-Ugriumov, L. P. Kotenko, E. P. Kuznetsov, and Iu. S. Popov, J. Exptl. Theoret. Phys. (U.S.S.R.) 34, 253 (1958) [translation: Soviet Phys.-JETP 34 (7), 176 (1958)].

With Scintillation Counters

M. Bardon, D. Berley, and L. M. Lederman, Phys. Rev. Letters 2, 56 (1959).

Marcel Weinrich, Study of Conservation Laws in the Pi-Mu-Electron Decay Chain, Columbia University doctoral dissertation, Feb. 1958 (unpublished).

A. I. Mukhin, E. B. Ozerov, and B. Pontecorvo, J. Exptl. Theor. Phys. 35 (8), 237 (1958).

J. M. Cassels, T. W. O'Keefe, M. Rigby, and J. Wormald, Proc. Phys. Soc. (London) 70, 543 (1957); Proc. Phys. Soc. (London) 72, 781 (1958).